0.1 μg of pCMV-hAR, 0.3 μg of pGL3-MMTV and 2 ng of pRL-CMV. The cells were then incubated with or without 10 nM DHT for 24 h and the luciferase activities were measured as described above.

2.5. Coimmunoprecipitation and immunoblot analysis

COS-7 or LNCaP cells (1×10^6 cells/dish) were seeded in 100 mm culture dishes and transiently transfected with 7.5 μg of a plasmid expressing GFP-tagged full-length TZF or its truncated mutants and 1.5 μg of pCMV-hAR, followed by incubation with or without 10 nM DHT for 24 h. The cells were lysed in a buffer consisting of 20 mM HEPES–NaOH, pH 7.9, 20% glycerol, 100 mM KCl, 0.2 mM EDTA, 0.5% NP-40 and a protease inhibitor cocktail (Roche Diagnostics, Tokyo, Japan) at 4 °C for 30 min, followed by a brief sonication. The lysates were collected by centrifugation. The protein concentrations were measured using a BCA protein assay kit (Pierce, Rockford, IL) and each protein concentration was adjusted to 1 mg/ml. For immunoprecipitation analyses, antibodies against green fluorescent protein (GFP) and AR (C-19) (Santa Cruz Biotechnology, Santa Cruz, CA) were preincubated with Protein A magnetic beads (New England Biolabs Inc., Beverly, MA) at 4 °C for 2 h. Each lysate (200 μg) was then incubated with 10 μg of the anti-GFP or -AR antibody-conjugated beads in WB buffer (20 mM HEPES–NaOH, pH 7.9, 20% glycerol, 100 mM KCl, 0.2 mM EDTA, 0.5% NP-40 and 0.5% skim milk) at 4 °C overnight. After the beads had been washed four times with 180 μl of WB buffer and four times with 180 μl of WH buffer (20 mM HEPES–NaOH, pH 7.9, 20% glycerol, 100 mM KCl, 0.2 mM EDTA and 0.5% NP-40), the bound proteins were eluted in 60 μl of 2× sodium dodecyl sulfate-polyacrylamide gel electrophoresis (SDS-PAGE) sample buffer (4% SDS, 200 mM dithiothreitol, 120 mM Tris–HCl, pH 6.8 and 0.02% bromophenol blue) and subjected to 10% SDS-PAGE at 20 mA for 4 h. Immunoblotting analyses were then performed as previously described (Kawate et al., 2005). Briefly, proteins were transferred onto a nitrocellulose membrane (Hybond ECL; Amersham Biosciences Corp., Piscataway, NJ) using a Hoefer miniVe unit (Amersham) at 250 V for 1 h at 25 °C. The membrane was blocked in 1× Block-Ace (Dainippon Pharmaceutical Co., Osaka, Japan) and reacted with an appropriate primary antibody in 0.1× Block-Ace for 1 h at 25 °C. Following a brief wash with TBS–Tween 20 (10 mM Tris–HCl, pH 8.0, 0.9% NaCl and 0.05% Tween 20), the membrane was incubated with a horseradish peroxidase-conjugated secondary antibody (Amersham) in 0.1× Block-Ace for 45 min at 25 °C. After washing with TBS–Tween 20, the membrane was reacted with ECL western blotting detection reagents (Amersham) and the bands were detected using a Versa-Doc Model 5000 Imaging System (Bio-Rad Laboratories, Hercules, CA).

2.6. HDAC activity assay

Polyclonal anti-TZF antibodies were obtained by subcutaneously injecting rabbits with 50 μg of the C-terminal 41 amino acids of TZF once per week for 4 weeks. COS-7 cells (1×10^6 cells/dish) were seeded in 100 mm culture dishes and transfected with 7 μg of pEGFP-TZF or pEGFP. After incubation for 24 h, cell lysates were prepared and incubated with the anti-TZF antibodies in the presence of Protein A magnetic beads. Immunoprecipitates were subjected to HDAC activity assays using an HDAC fluorescent activity assay kit (AK-500; Biomol Research Laboratories, Plymouth Meeting, PA) according to the manufacturer's recommended protocol. The beads were resuspended in 100 μl of 250 μM Fluor de Lys substrate in the presence or absence of 5 μM TSA and incubated with rocking at 25 °C for 90 min. Next, 25 μl of each reaction mixture was added to 25 μl of assay buffer (25 mM Tris–HCl, pH 8.0, 137 mM NaCl, 2.7 mM KCl and 1 mM $MgCl_2$) and 50 μl of 1× Fluor de Lys Developer with 2 μM TSA, and incubated for 15 min at 25 °C to stop the HDAC reaction. The HDAC activities were measured by excitation with 360 nm light and emission of 460 nm light using an ARVO SX 1420 multilabel counter (Wallac, Turku, Finland).

2.7. Confocal laser scanning microscopy

For living cell microscopy, COS-7 cells (2×10^5 cells/dish) were cultured in 35 mm glass-base dishes (Asahi Techno Glass Corp., Tokyo, Japan) and transfected with pAR-GFP or pAR-CFP and GFP (YFP)-tagged full-length TZF or its truncated mutants using Superfect reagents (Qiagen). After incubation for 3 h, the cells were washed with PBS, maintained in DMEM supplemented with 10% charcoal-treated FBS for 16–20 h and then incubated in the presence or absence of 10 nM DHT. The cells were observed with an Axiovert 200M inverted microscope equipped with an LSM 510 META scan head (Carl Zeiss Co. Ltd., Jena, Germany) using a 100× 1.4 numerical aperture oil immersion objective as described previously (Kawate et al., 2005). Images were collected at a 12-bit depth resolution of intensities over 1024 × 1024 pixels. For excitation of CFP, GFP and YFP, 458 and 488 nm argon lasers were employed and the emission signals were separated using the emission fingerprinting technique established by Carl Zeiss. Separation of the individual emission signals was based on recordings of the spectral signature of each emission signal and a digital unmixing procedure using these reference spectra. A three-dimensional imaging study was performed as previously described (Saitoh et al., 2002). Briefly, a series of 30–50 two-dimensional images were collected for each nucleus using a confocal laser microscope, and reconstructed using the three-dimensional analysis software of the TRI Graphics Program (Ratoc System Engineering, Tokyo, Japan). Both the spatial distribution and calculation of the fluorescent proteins as distinct volumes were made possible by removing scattering background fluorescence and lens spherical aberrations and then separating each particle. The analytical conditions were kept constant throughout all the experiments. The numbers of subnuclear foci were representative of at least 15 cells.

2.8. Immunostaining

COS-7 cells (2×10^4 cells/well) were seeded in Lab-Tek II Chamber Slides (Nalge Nunc International, Naperville, IL) and transfected with pEGFP-TZF using 1 μl/well of the Superfect reagent. After incubation for 24 h, the cells were washed with PBS and fixed with 50% methanol/50% acetone for 10 min at −20 °C. After blocking in 1× Block-Ace for 10 min at 25 °C, the cells were incubated with an anti-HDAC2 goat polyclonal IgG antibody (Santa Cruz; 1:200 dilution in 0.1× Block-Ace) for 1 h at 25 °C. Following a brief wash with TBS–Tween 20, the cells were incubated with Alexa Fluor 546-conjugated donkey anti-goat IgG (H+L) (Molecular Probes Inc., Eugene, OR; 1:400 dilution in 0.1× Block-Ace) for 1 h at 25 °C. After washing with TBS–Tween 20, the cells were mounted in Vectashield (Vector Laboratories, Burlingame, CA) and observed under a confocal laser scanning microscope using 488 nm (argon) and 543 nm (helium-neon) laser lines for excitation of GFP and Alexa Fluor 546, respectively.

2.9. Fluorescence recovery after photobleaching (FRAP) analysis

COS-7 cells (2×10^5 cells/dish) were seeded in 35 mm glass-base dishes and transfected with various plasmids as described above. After addition of the ligand, FRAP analysis was performed by confocal laser scanning microscopy essentially as previously described (Stenoien et al., 2001). After collection of the initial image, a selected area of a fixed size (region of interest, ROI) in the nucleus was photobleached using the maximum power of the 488 nm argon laser for 70 iterations. After the bleaching, images were taken every 0.5 s at a resolution of 256 × 256 pixels to follow the recovery of the fluorescence intensity in the ROI. The fluorescence intensities of the ROI were calculated using the LSM software and the half-recovery time ($t_{1/2}$) was determined using the Microsoft Excel software.

3. Results

3.1. A central domain of TZF is required for repression of AR-mediated transactivation

Using different promoters and cells, we confirmed that AR-mediated transactivation was repressed by TZF in a dose-dependent manner (Fig. 1A and B). Endogenous AR-mediated transactivation was also inhibited by expression of TZF (Fig. 1B). To determine the repression domain in the TZF protein, various TZF deletion mutants were constructed (Fig. 2A) and subjected to functional promoter assays in COS-7

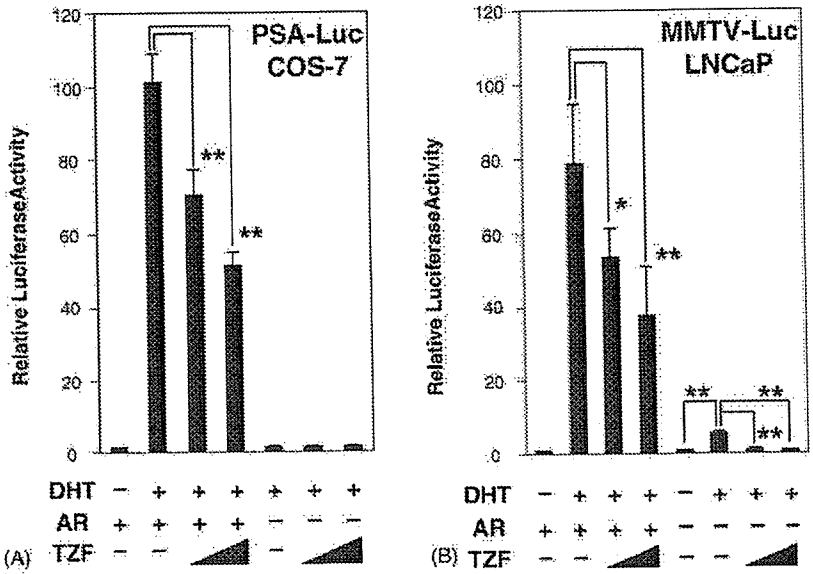

Fig. 1. Repression of AR-mediated transactivation by TZF. COS-7 (A) and LNCaP (B) cells were cotransfected with pGL3-PSA (A) or pGL3-MMTV (B) as a reporter and pRL-CMV as an internal control, with or without pCMV-hAR and pFLAG-CMV2-TZF. The amounts of the transfected plasmids were described in Section 2, except for the use of 0.5 or 1.0 μg of pFLAG-CMV2-TZF. The cells were incubated in the absence or presence of 10 nM DHT for 24 h and the luciferase activities were measured. The right-hand three bars in (A) and four bars in (B) show the results of control cells without transfection of the AR expression vector. Bars show the fold change in the luciferase activity relative to the value induced by AR without DHT. The data represent the means ± S.D. of three independent experiments. $^{*}P<0.05$; $^{**}P<0.01$.

cells (Fig. 2B and C). The TZF(1–275) mutant, consisting of the N-terminal region of TZF, was unable to repress AR-mediated transactivation, whereas TZF(275–942) lacking the N-terminal region showed the same level of repression as full-length TZF (Fig. 2B). These results indicate that the N-terminus is not involved in the repression function of TZF. Surprisingly, two other truncated mutants of TZF, namely TZF(1–663) and TZF(512–942), showed much stronger repression of AR-mediated transactivation than wild-type TZF (Fig. 2B). Since the common amino acid sequence between these two strong mutants consisted of residues 512–663, we examined the effects of TZF(512–663) comprising these amino acids and TZF(Δ512–663) lacking these amino acid residues on the transactivation activity for AR (Fig. 2A). As shown in Fig. 2C, TZF(512–663) repressed AR-mediated transcriptional activation as strongly as TZF(1–663) and TZF(512–942), whereas TZF(Δ512–663) had no effect. These results indicate that amino acid residues 512–663 are essential for the repressive effect of TZF on AR-mediated transactivation.

3.2. Interaction between the central domain (512–663) of TZF and AR

To examine whether the TZF(512–663) domain could interact with AR, modified mammalian one-hybrid assays were performed. In this system, expression plasmids for AR and VP16-fused proteins of interest were cotransfected with an MMTV promoter-luciferase reporter plasmid into NIH3T3 cells. If the protein of interest was able to interact with AR, transactivation would be enhanced compared to the basic activity of AR without the VP16-fused protein. Although the N-terminus of TZF, TZF(1–275), was unable to enhance the transactivation, full-length TZF, TZF(1–663) and TZF(512–663) enhanced the reporter activity, indicating that these three proteins were able to interact with AR (Fig. 3B). The internal deletion mutant TZF(Δ512–663) was unable to enhance the luciferase activity (Fig. 3B).

We previously demonstrated that full-length TZF coimmunoprecipitated with AR (AR-AF-1 domain) (Ishizuka et al., 2005). Therefore, coimmunoprecipitation analyses were performed to investigate the interaction between AR and the truncated TZF mutants. GFP-tagged full-length TZF or its truncated mutants and AR were coexpressed in COS-7 cells, and cell extracts were immunoprecipitated with an anti-AR or anti-GFP antibody. As shown in Fig. 4, AR was coimmunoprecipitated with full-length TZF and TZF(512–663), but not with TZF(Δ512–663). These results further confirm that TZF(512–663) is able to interact with AR.

3.3. HDAC activity is involved in the TZF-repression complex

HDAC activity is often identified in corepressor complexes associated with steroid hormone receptors. To investigate whether HDAC activity is related to the TZF-induced repression of AR transactivation, COS-7 cells were treated with TSA, a specific inhibitor of HDAC, and subjected to functional promoter assays. As shown in Fig. 5A, ligand-dependent AR transactivation was enhanced after TSA treatment. Although coexpression of TZF repressed AR-mediated transactivation, TSA completely

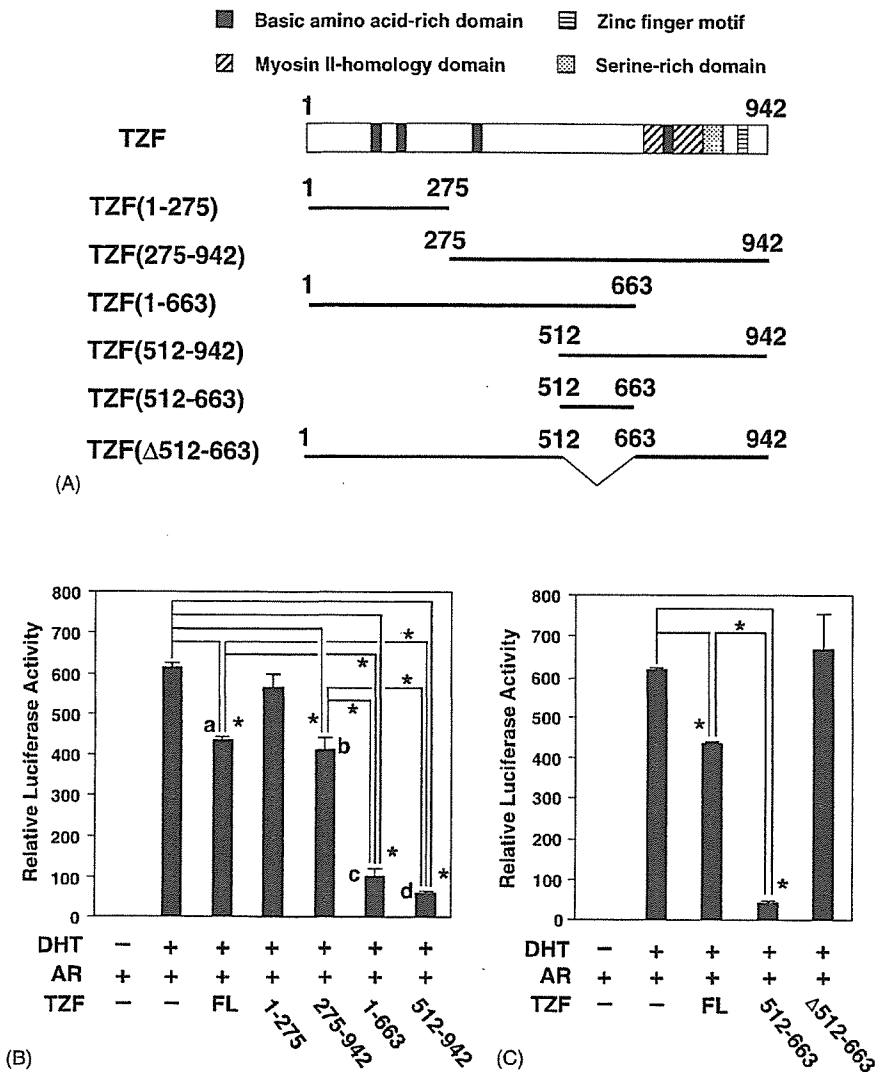

Fig. 2. Identification of the repression domain in TZF for AR-mediated transactivation. (A) Schematic representation of full-length TZF and its various truncated mutants. Several conserved domains including a zinc finger motif are indicated. (B) Effects of full-length TZF and its truncated mutants on AR-mediated transactivation. (C) The TZF(512–663) domain is required for the repression of AR-mediated transactivation by TZF. COS-7 cells were transiently transfected with pGL3-MMTV, pRL-CMV, pCMV-hAR and an expression plasmid for full-length TZF (FL) or its truncated mutants as described in Section 2. The transfected cells were incubated with or without 10 nM DHT for 24 h and the luciferase activities were measured. Bars show the fold change in the luciferase activity relative to the value induced by AR without DHT. The data represent the means ± S.D. of three independent experiments. $^{*}P<0.01$. a and b > c and d ($P<0.01$).

abolished this effect (Fig. 5A). We further tested whether the strong repressive effect of TZF(512–663) was influenced by TSA. As shown in Fig. 5B, TSA was able to reverse the repression by TZF(512–663) in a dose-dependent manner. To further confirm HDAC involvement in the TZF-repression complex, TZF was immunoprecipitated by an anti-TZF antibody and the immunoprecipitate was subjected to an HDAC activity assay. The immunoprecipitate from the TZF-expressing cells showed remarkably higher HDAC activity than that from cells without expression of TZF. Abolishment of the HDAC activity by TSA confirmed that the TZF-immunocomplex contained HDAC activity (Fig. 5C). These results indicate that HDAC activity is involved in the TZF-induced repression of AR-mediated transactivation.

To investigate which HDAC protein is involved in the TZF-induced repression of AR, immunoblot analyses with several anti-HDAC antibodies were performed on immunoprecipitates pulled down by an anti-GFP antibody from GFP-TZF expressing COS-7 cells. The results revealed that HDAC2 was coimmunoprecipitated with TZF (Fig. 6A), whereas HDAC1 and HDAC3 were not (data not shown). To examine the intracellular localization of HDAC2, GFP-TZF-expressing COS-7 cells were immunostained with an anti-HDAC2 antibody. Endogenous HDAC2 was located in the nucleus where it formed discrete dots that were colocalized with TZF (Fig. 6B). These data indicate that TZF probably interacts with HDAC2 in the cells. We further found that TZF was able to interact with AR and HDAC2. To investigate whether these three proteins were involved in the

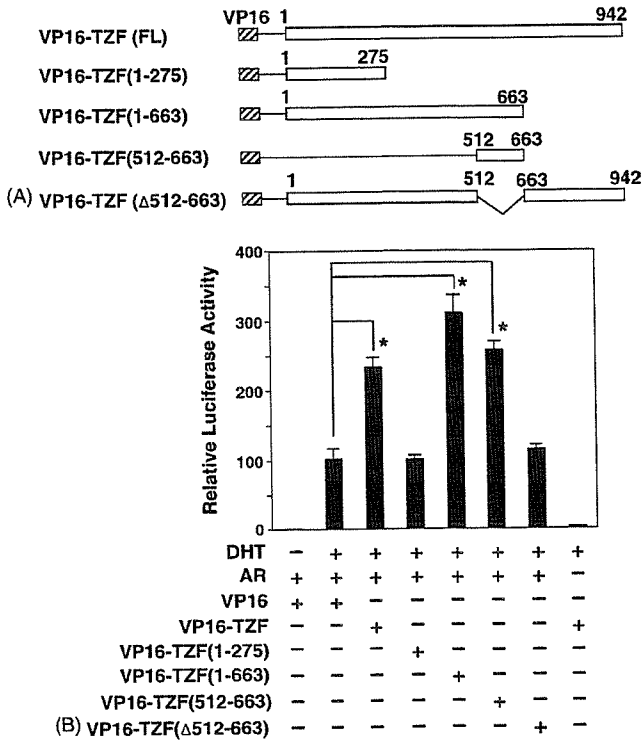

Fig. 3. Identification of the interaction domain of TZF with AR by a modified mammalian one-hybrid assay. (A) Schematic representation of VP16-fused full-length TZF (FL) and its truncated mutants. (B) A central domain (amino acids 512–663) of TZF can interact with AR. NIH3T3 cells were cotransfected with pCMV-hAR, pGL3-MMTV, pRL-CMV and an expression plasmid for VP16-fused TZF or its truncated mutants as indicated. The cells were incubated with or without 10 nM DHT for 24 h and the luciferase activities were measured. Bars show the fold change in the luciferase activity relative to the value induced by VP16 and AR without DHT. The data represent the means ± S.D. of three independent experiments. $^{*}P < 0.01$.

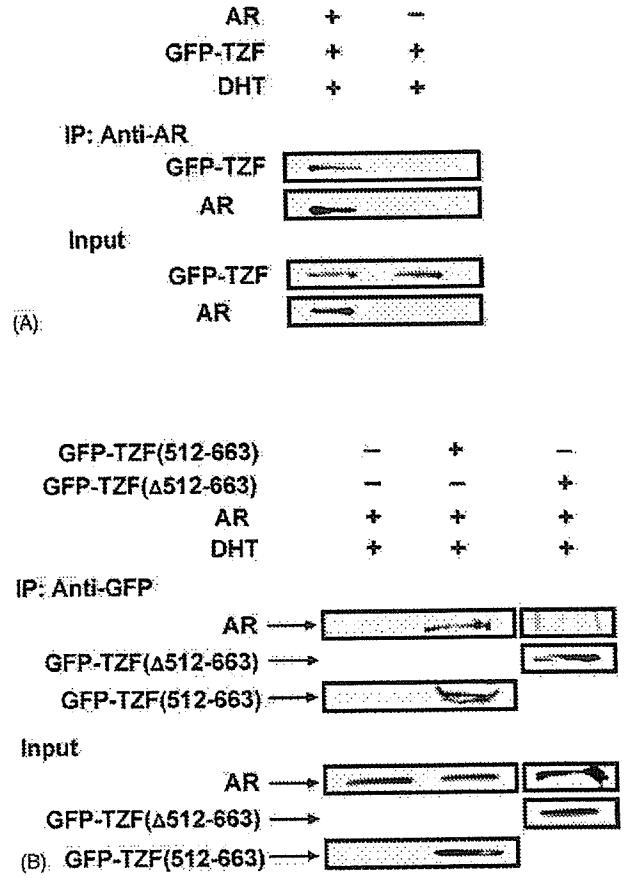

Fig. 4. Coimmunoprecipitation analyses of TZF and its truncated mutants with AR. (A) Coimmunoprecipitation of full-length TZF with AR. COS-7 cells were transfected with pEGFP-TZF and pCMV-hAR or an empty vector and incubated with 10 nM DHT for 24 h. Whole cell lysates were immunoprecipitated using an anti-AR antibody. (B) Coimmunoprecipitation of truncated TZF mutants with AR. COS-7 cells were cotransfected with pCMV-hAR and pEGFP-TZF(512–663), pEGFP-TZF(Δ512–663) or an empty vector, and treated with 10 nM DHT for 24 h. Whole cell lysates were immunoprecipitated using an anti-GFP antibody. The precipitates were subjected to immunoblot analyses using an anti-AR antibody for detection of AR and an anti-GFP antibody for detection of TZF and its mutants tagged with GFP. The expression levels of AR, TZF and the truncated TZF proteins were confirmed by immunoblot analyses of the whole cell lysates.

same protein complex, coimmunoprecipitation analyses were performed using LNCaP cells expressing endogenous AR and HDAC2. After transfection of pEGFP-TZF or an empty vector, LNCaP cells were incubated with DHT and the whole cell extract was prepared for immunoprecipitation with an anti-GFP antibody. Immunoblot analysis revealed that endogenous AR and HDAC2 were coimmunoprecipitated with GFP-TZF (Fig. 6C). These results indicate that AR, TZF and HDAC2 form a ternary complex during the repression of AR-mediated transactivation.

3.4. Ligand-dependent intranuclear colocalization of TZF or its truncated mutants with AR

As reported in our previous studies using GFP-fused proteins and confocal laser microscopy (Tomura et al., 2001; Saitoh et al., 2002), AR was located in the cytoplasm in the absence of the ligand, and translocated into the nucleus to form uniform fine foci after ligand addition in COS-7 cells (Fig. 7Aa and Ab). On the other hand, TZF was localized in the nucleus where it formed discrete dots that were larger and less numerous than the ligand-induced AR foci (Fig. 7Ac). Interestingly, upon coexpression of non-fluorescent AR, the TZF dot pattern was completely changed after DHT addition and became similar to the AR foci pattern (Fig. 7Ad and Ae) as previously reported (Ishizuka et al., 2005). Using different fluorescent proteins (GFP and YFP), colocalization of these two proteins was confirmed (Fig. 7B). Thus, TZF was considered to be recruited into AR foci in a ligand-dependent manner. To examine the colocalization of TZF mutants with AR, AR and TZF mutants fused to different fluorescent proteins were coexpressed and observed under a confocal microscope. TZF(1–275) lacking the repressive effect on AR-mediated transactivation was diffusely distributed in the nucleus in the absence of the ligand. After addition of DHT, AR was translocated into the nucleus to form fine foci but TZF(1–275) remained diffuse in the nucleus and did not colocalize with AR (Fig. 7C). TZF(1–663), which repressed AR-mediated transactivation more strongly

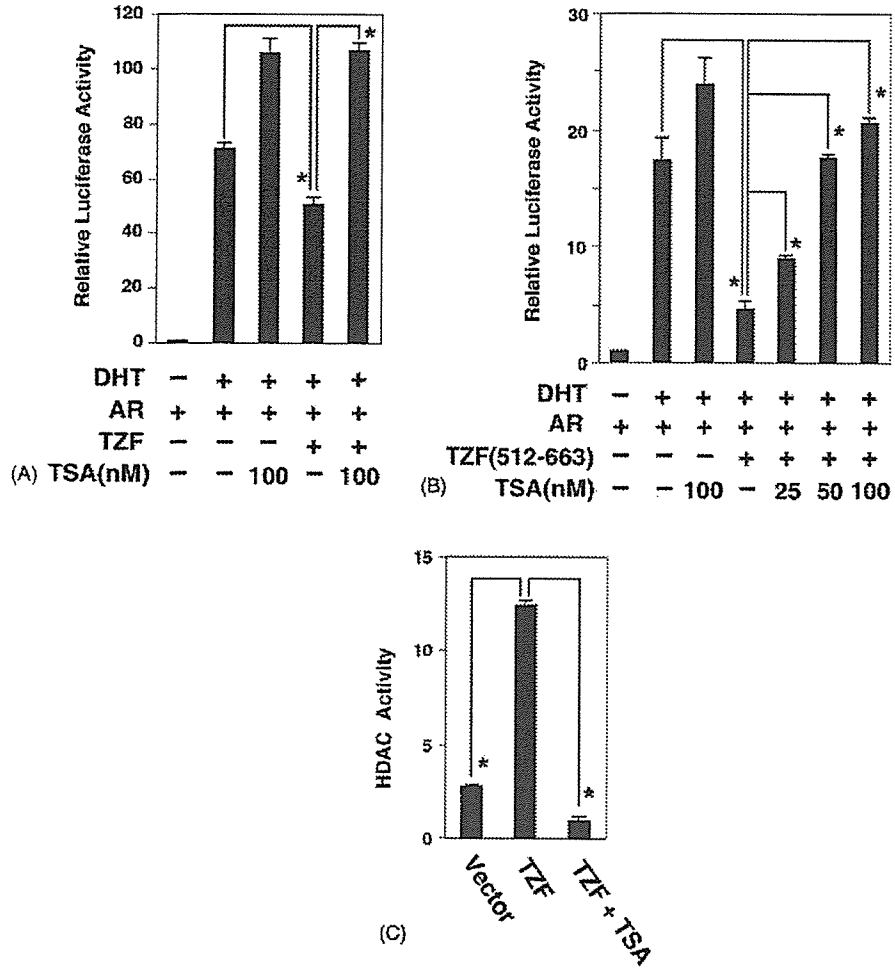

Fig. 5. HDAC activity is involved in TZF-induced repression of AR-mediated transactivation. (A) Repression of AR-mediated transactivation by TZF is recovered by TSA. (B) TZF(512–663)-induced repression of AR-mediated transactivation is recovered by TSA in a dose-dependent manner. COS-7 cells were transiently transfected with pGL3-PSA, pRL-CMV and pCMV-hAR, with or without pFLAG-CMV2-TZF (A) or pFLAG-CMV2-TZF(512–663) (B) as described in Section 2. The cells were incubated in the absence or presence of 10 nM DHT for 12 h and then left untreated or treated with TSA as indicated, followed by incubation for an additional 12 h. Next, whole cell extracts were prepared and subjected to luciferase assays. Bars show the fold change in the luciferase activity relative to the value induced by AR without DHT. The data represent the means ± S.D. of three independent experiments. $^{*}P<0.01$. (C) TZF-immunocomplexes contain HDAC activity. COS-7 cells were transiently transfected with pEGFP or pEGFP-TZF. After incubation for 24 h, whole cell lysates were prepared and immunoprecipitated with an anti-TZF antibody. The precipitates were subjected to HDAC activity assays as described in Section 2. The data represent the means ± S.D. of three independent experiments. $^{*}P<0.01$.

than wild-type TZF, showed a ligand-induced change in the pattern of its intranuclear dots, similar to the case for wild-type TZF. The nuclear dots of TZF(1–663) became smaller and more numerous and were colocalized with AR (Fig. 7D). TZF(512–663) also strongly repressed AR-mediated transactivation, but this mutant was diffusely distributed in both the nucleus and the cytoplasm and did not form intranuclear dots in the absence of DHT (Fig. 7E, upper panels). In the presence of the ligand, fluorescent signals for TZF(512–663) were only observed in the nucleus where they were colocalized with AR (Fig. 7E, lower panels). These colocalization results are consistent with the above-described results for the modified mammalian one-hybrid assays and coimmunoprecipitation experiments.

3.5. Correlation of the intranuclear foci number of AR with its transactivation activity

Although ligand treatment caused colocalization of TZF(512–663) with AR, the distinct intranuclear foci formation of AR seemed to be inhibited by this mutant (Fig. 7Ab and Ee), which showed strong repression of AR-mediated transactivation (Fig. 2C). These results suggested that the transactivation function of AR may be related to the number of its distinct intranuclear foci. To prove this hypothesis, we first quantified the number of intranuclear AR foci in COS-7 cells using three-dimensional images reconstructed from tomographic images collected by a confocal microscope. This method is able to detect a distinct volume by removing

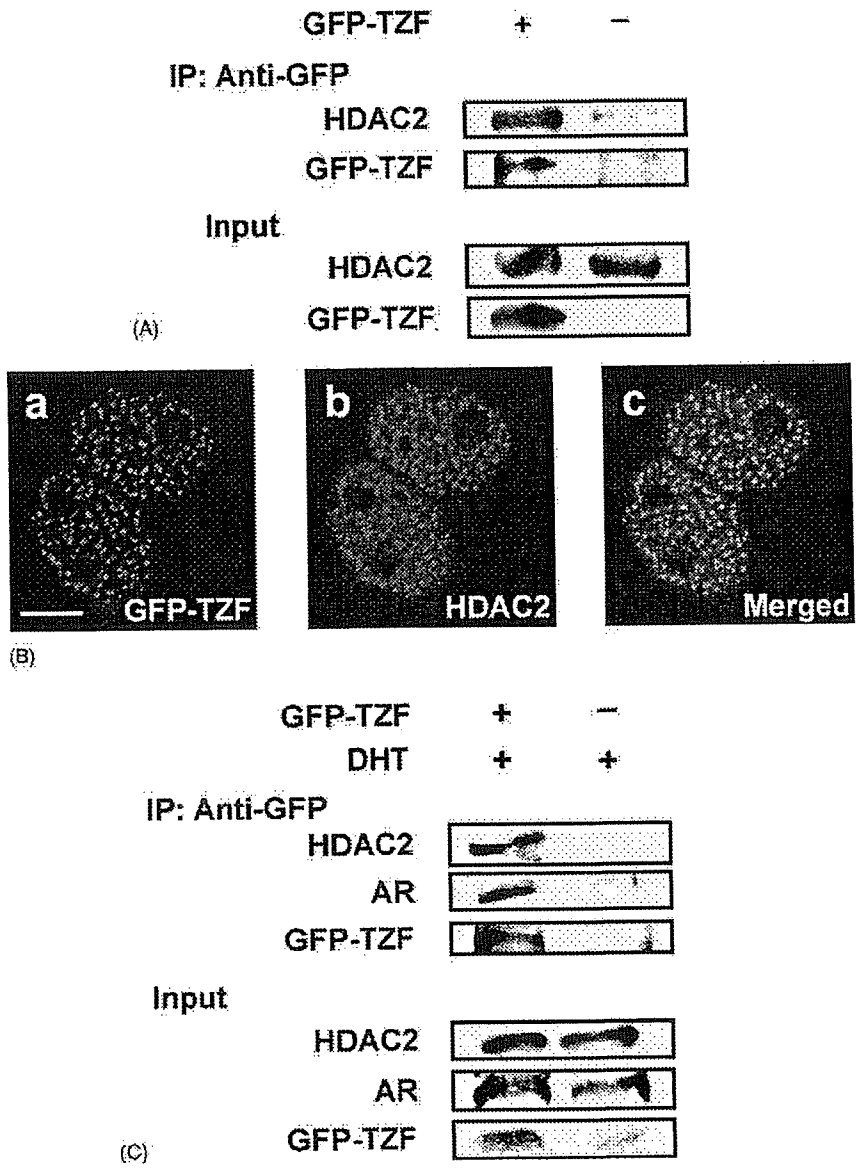

Fig. 6. HDAC2 is involved in the TZF repression complex. (A) Endogenous HDAC2 is coimmunoprecipitated with TZF. COS-7 cells were transiently transfected with pEGFP-TZF or an empty vector and incubated for 24 h. Whole cell lysates were immunoprecipitated with an anti-GFP antibody. The precipitates were subjected to immunoblot analyses with an anti-HDAC2 antibody for detection of endogenous HDAC2 and an anti-TZF antibody for detection of GFP-TZF. To confirm the expression levels of endogenous HDAC2 and transfected GFP-TZF, the whole cell lysates were directly subjected to the immunoblot analyses. (B) Colocalization of TZF with endogenous HDAC2. COS-7 cells were transiently transfected with pEGFP-TZF and incubated for 24 h. The cells were fixed and immunostained with an anti-HDAC2 antibody, followed by incubation with an Alexa Fluor 546-labeled secondary antibody. Signals for GFP-TZF (green; a) and HDAC2 (red; b) were observed by laser confocal microscopy, and the two signals were merged (c). Bar = 5 μm. (C) Endogenous AR and HDAC2 are both involved in TZF-immunocomplexes in LNCaP cells. LNCaP cells were transiently transfected with pEGFP-TZF or an empty vector and incubated in the presence of 10 nM DHT for 48 h. Whole cell lysates were immunoprecipitated with an anti-GFP antibody. The precipitates were subjected to immunoblot analyses with an anti-HDAC2 antibody for detection of HDAC2, an anti-AR antibody for detection of AR and an anti-GFP antibody for detection of GFP-TZF. To confirm the expression levels of endogenous HDAC2, AR and GFP-TZF, the whole cell lysates were also subjected to the immunoblot analyses (for interpretation of the references to colour in this figure legend, the reader is referred to the web version of the article).

background scattering fluorescence and relatively diffusely distributed fluorescence, thereby clearly showing a difference in the intranuclear spatial distribution of the foci. The number of ligand-induced intranuclear foci of AR was 317 ± 58 ($n = 15$) (Fig. 8Aa) and this was not influenced by coexpression of an empty vector, pFLAG-CMV2 or pcDNA3 (315 ± 42, $n = 18$) (Fig. 8Ab). When AR and TZF(512–663) were coexpressed at a ratio of 1:1.5, the number of AR foci was decreased to 189 ± 53 ($n = 15$) (Fig. 8Ac). Furthermore, increased TZF(512–663) at a ratio of 1:10 almost completely inhibited the AR foci formation (22 ± 16, $n = 18$) (Fig. 8Ad). Next, we tested the effect of a coactivator protein, TIF2, on the number of intranuclear AR foci. Initially, AR, TZF(512–663) and TIF2 were coexpressed at a ratio of 1:10:3. As shown in Fig. 8Ae, TIF2 expres-

sion partially recovered the number of intranuclear AR foci (101 ± 18, $n = 18$). Coexpression of an equal amount of TIF2 to TZF(512–663) at a ratio of 1:10:10 completely recovered the number of intranuclear AR foci to the basal level without the TZF mutant (318 ± 44, $n = 18$) (Fig. 8Af). The corepressor TZF(512–663) decreased the number of intranuclear AR foci, and the coactivator TIF2 was able to reverse this inhibition of AR foci formation. To compare the number of intranuclear AR foci with the transcriptional activity, functional promoter assays were performed using the same transfection conditions used for the experiments in Fig. 8A. TZF(512–663) repressed ligand-dependent AR-mediated transactivation in a dose-dependent manner (Fig. 8B). When AR and TZF(512–663) were coexpressed with TIF2 at a ratio of 1:10:3, AR-mediated

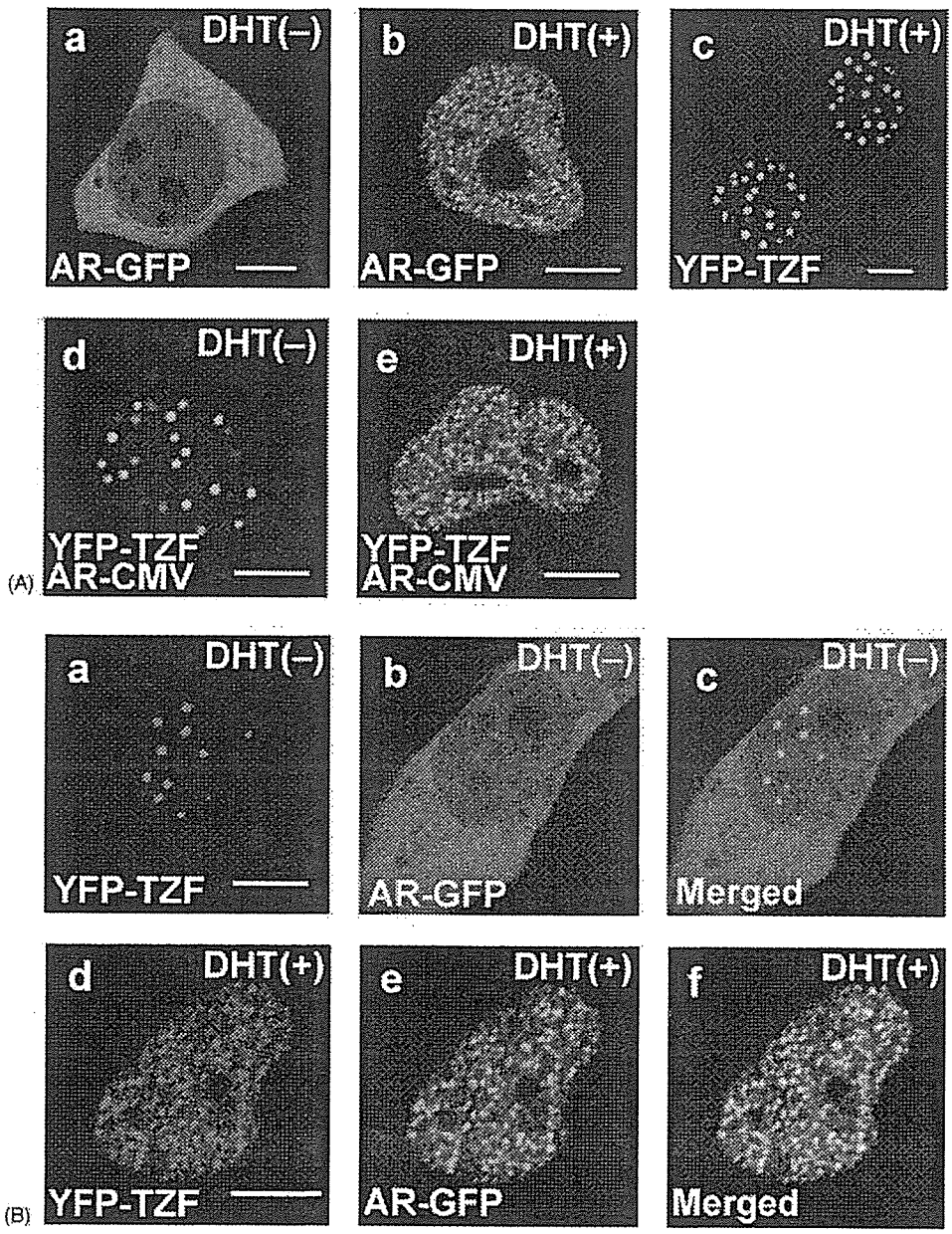

Fig. 7. Subcellular localizations of AR, full-length TZF and truncated TZF mutants. (A) Subcellular localizations of AR and TZF. COS-7 cells were transfected with pAR-GFP alone (a and b), pEYFP-TZF alone (c) or both pEYFP-TZF and pCMV-hAR (d and e) and incubated for 24 h. After incubation with or without 10 nM DHT for 1 h, the cells were observed under a laser confocal microscope. (B–E) Analyses of AR colocalization with TZF or its truncated mutants. COS-7 cells were cotransfected with pAR-GFP/CFP and pEYFP-TZF (B), pEYFP-TZF(1–275) (C), pEYFP-TZF(1–663) (D) or pEGFP-TZF(512–663) (E). The amounts of the transfected plasmids were the same as those in the functional promoter assay described in Section 2. The cells were incubated for 24 h and then further incubated in the absence (upper panels, a–c) or presence (lower panels, d–f) of 10 nM DHT for 1 h before observation by laser confocal microscopy. a and d, signals from TZF or its mutants (red); b and e, signals from AR (green); c and f, merged signals. Bars = 5 μm (for interpretation of the references to colour in this figure legend, the reader is referred to the web version of the article).

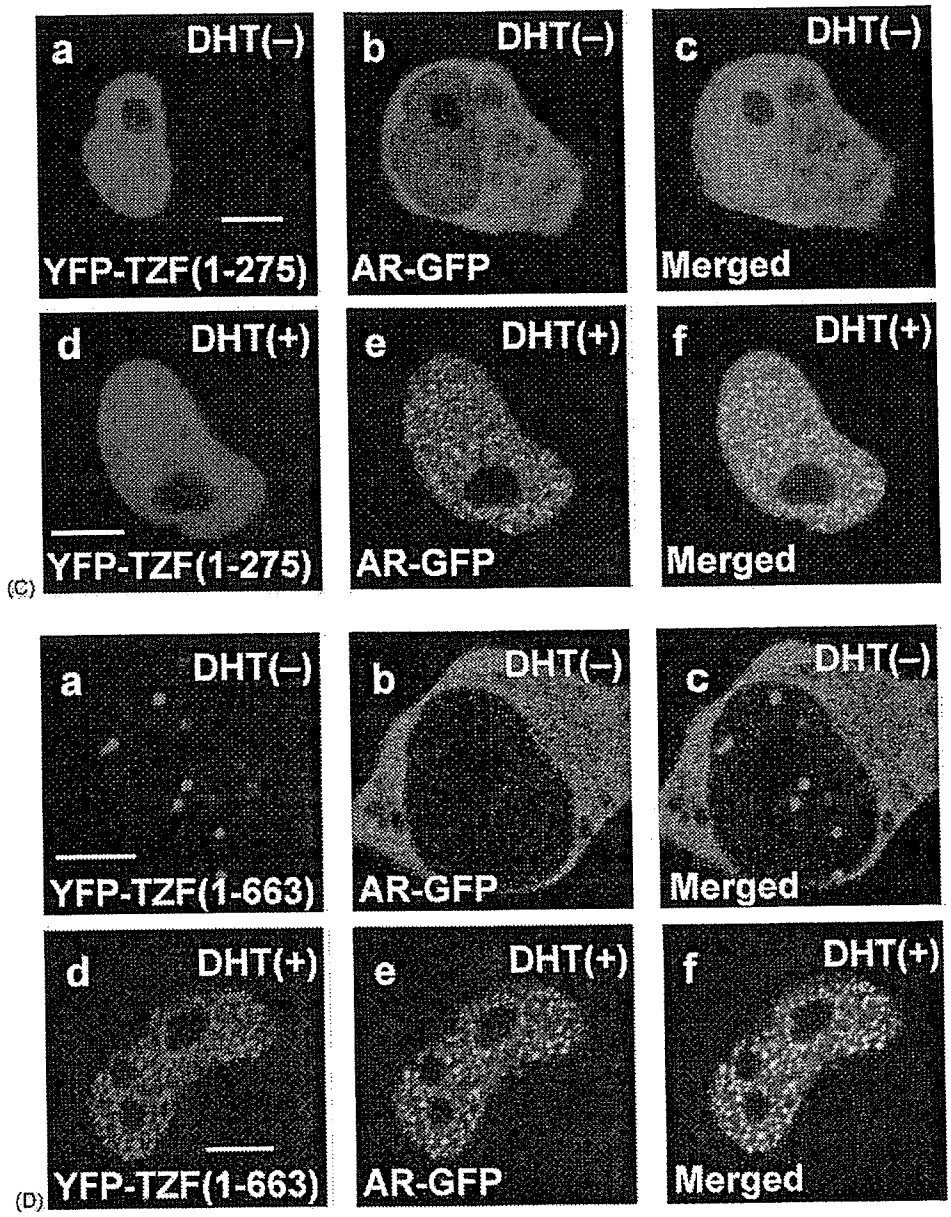

Fig. 7. (*Continued*).

transactivation was partially recovered. Moreover, when TIF2 was coexpressed at an equal level to TZF(512–663) at a ratio of 1:10:10, AR-mediated transactivation was recovered to almost the same level as that for DHT-bound AR alone (Fig. 8B). These data provide powerful evidence for our previous speculation that AR foci formation is closely linked to its transactivation function (Tomura et al., 2001; Saitoh et al., 2002).

3.6. TIF2 is released from AR foci by coexpression of TZF

To further analyze the competition between TIF2 and TZF for AR foci formation, the effect of TZF on the intranuclear localization of TIF2 was evaluated using COS-7 cells expressing YFP-TIF2 and AR-GFP with or without cotransfection of pFLAG-CMV2-TZF. In the absence of the ligand, TIF2 formed discrete dots in the nucleus and AR was located in the cytoplasm (Fig. 9a–c). After addition of the ligand, the discrete dots of TIF2 disappeared and it was recruited into the intranuclear AR fine foci (Fig. 9d–f). The almost complete colocalization of AR and TIF2 is characterized by the yellow color of the merged image in Fig. 9f. However, coexpression of TZF released TIF2 from the AR foci, even in the presence of DHT, and the discrete TIF2 dots reappeared (Fig. 9g–i). The green signals of AR and red signals of TIF2 were clearly separated (Fig. 9i). Conversely, the colocalization of TZF with AR (Fig. 9j–l) was impaired by coexpression of TIF2 (Fig. 9m–o) and the original TZF dots reappeared (Fig. 9n). The green signals of AR and red signals of TZF were clearly separated (Fig. 9o). These results suggest that TIF2 and TZF compete for interaction with AR in the cells.

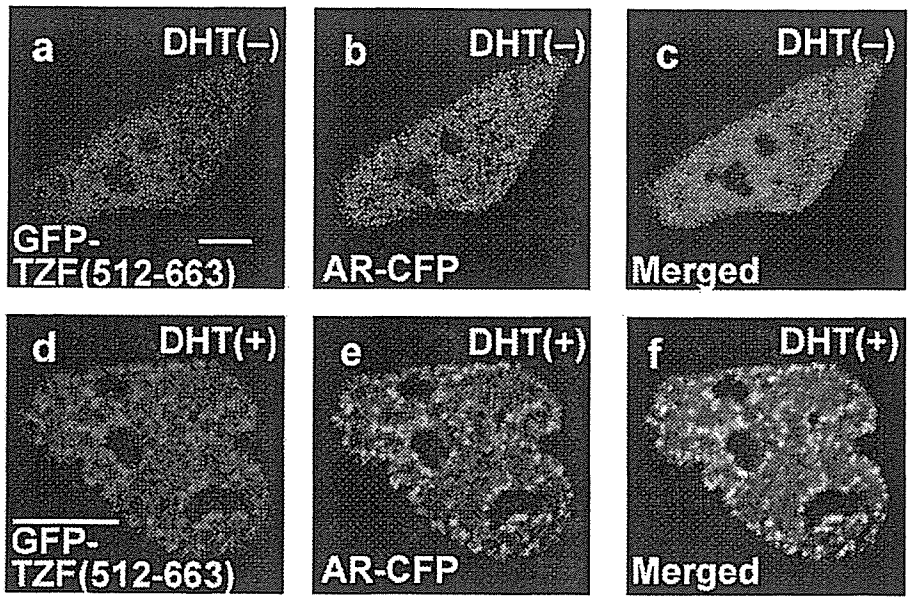

Fig. 7. (*Continued*).

3.7. Effects of TZF and TZF(512–663) on the intranuclear dynamics of AR

Previous FRAP analyses revealed that steroid hormone receptors show decreased intranuclear mobility after ligand treatment due to their association with the nuclear matrix, which is essential for ligand-induced transcriptional activation (Stenoien et al., 2001; Schaaf and Cidlowski, 2003). To examine the effects of TZF and TZF(512–663) on the intranuclear mobility of AR, FRAP experiments were performed using a confocal microscope in COS-7 cells. After treatment with DHT for 1 h, a ROI was photobleached using the maximal power of a 488 nm argon laser. After the photobleaching, images were taken every 0.5 s and the normalized fluorescence intensities of the ROI were calculated and plotted against time. In the presence of the ligand, AR-GFP-expressing cells showed fluorescence recovery and the half-recovery time was 7.5 ± 0.9 s ($n = 20$) (Fig. 10, upper panel). In this experiment, the bleached ROI could still be distinguished from unbleached regions even at 30 s after the photobleaching (Fig. 10, upper panel). Upon coexpression of full-length TZF, the bleached ROI became unclear at 30 s after the photobleaching and the half-recovery time (5.5 ± 0.9 s, $n = 15$) was shorter than that for AR alone (Fig. 10, middle panel). Furthermore, coexpression of TZF(512–663) showed much faster recovery ($t_{1/2} = 3.2 \pm 0.5$ s, $n = 15$) (Fig. 10, lower panel). These results suggest that the intranuclear mobility of AR is increased by coexpression of TZF or TZF mutants that may weaken the interaction of AR with the nuclear matrix.

4. Discussion

The mechanism of TZF-induced repression of AR-mediated transactivation was further examined in the present study. Luciferase reporter (Fig. 2C), modified mammalian one-hybrid (Fig. 3B) and coimmunoprecipitation (Fig. 4B) assays using truncated mutants of TZF clearly demonstrated that a central portion (amino acids 512–663) of TZF is responsible for both binding to AR and repressing AR-mediated transactivation. Corepressor complexes containing N-CoR and SMRT are considered to recruit HDAC and then repress transcription (Jones and Shi, 2003). TZF also recruits endogenous HDAC2 and forms a complex with endogenous AR in the presence of DHT (Figs. 5C, 6B and 6C), and the specific HDAC inhibitor TSA completely prevented the transcriptional repression by TZF (Fig. 5A–C), suggesting that recruitment of HDAC2 into the AR/TZF complex is the major mechanism of the repression. Two of the truncated TZF mutants, namely TZF(1–663) and TZF(512–942), repressed AR-mediated transactivation much more strongly than full-length TZF, and a similar level of repression was observed for their common region, TZF(512–663). Based on these results, it may be speculated that the central portion (amino acids 512–663) is structurally positioned inside the TZF molecule, such that removal of the N- or C-terminal of the molecule may cause further exposure of the active domain, thereby resulting in a stronger interaction and repression of transactivation. TZF(512–663) does not contain a CoRNR motif (I/LXXII), which has been found in the corepressors N-CoR and SMRT and is considered to be sufficient for both their interactions with nuclear receptors and repression of transactivation (Webb et al., 2000; Hu et al., 2001). To examine whether TZF(512–663) contains some specific secondary structures, a protein structure prediction analysis was performed on this region (PredictProtein; Columbia University Bioinformatics Center, New York, NY). Although no regular secondary structures (helices, strands or coiled-coils) were found in this region, such a long region without any regular secondary structures is categorized into non-regular secondary structure (NORS), which indicates a structurally flexible region. NORS regions

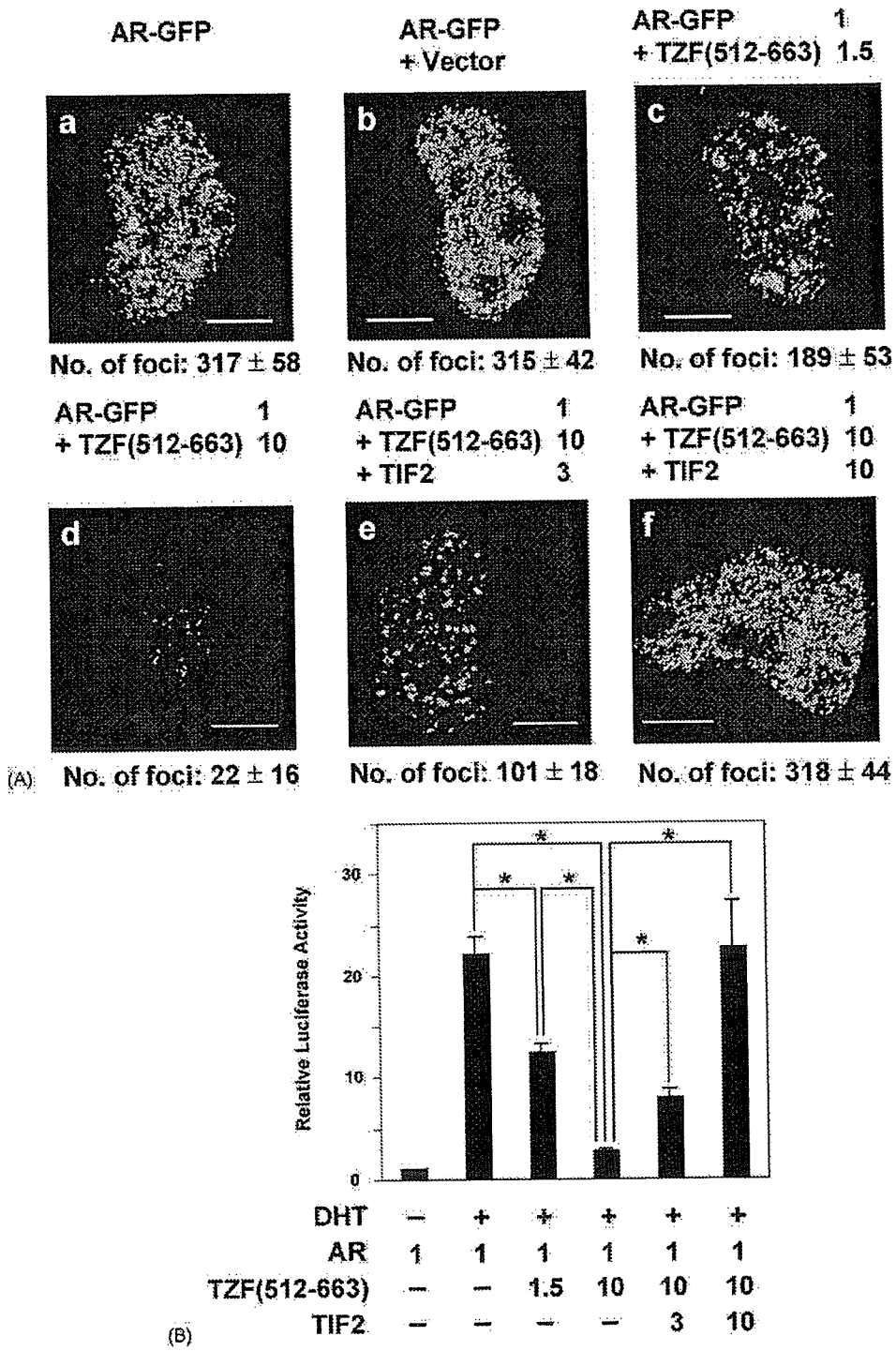

Fig. 8. The number of intranuclear AR foci is correlated with its transactivation activity. (A) Three-dimensional imaging analyses of the intranuclear AR foci. COS-7 cells were transiently transfected with 1 μg of pAR-GFP alone (a) or together with an empty vector (b), 1.5 μg of pFLAG-CMV2-TZF(512–663) (c), 10 μg of pFLAG-CMV2-TZF(512–663) (d), 10 μg of pFLAG-CMV2-TZF(512–663) and 3 μg of pcDNA-TIF2 (e) or 10 μg of pFLAG-CMV2-TZF(512–663) and 10 μg of pcDNA-TIF2 (f). The cells were incubated for 24 h and treated with 10 nM DHT for 1 h before observation. Two-dimensional tomographic images were collected by a confocal laser scanning microscope and reconstructed as described in Section 2. The number of subnuclear foci was calculated from at least 15 cells for each transfection and is shown as the mean ± S.D. below each panel. Bars = 5 μm. (B) Effects of TZF(512–663) and TIF2 on AR-mediated transcriptional activation. COS-7 cells were transiently transfected with 0.3 μg of pGL3-MMTV, 2 ng of pRL-CMV and 0.1 μg of pAR-GFP, together with various combinations of 0.15 or 1 μg of pFLAG-CMV2-TZF(512–663) and 0.3 or 1 μg of pcDNA-TIF2. After incubation with or without 10 nM DHT for 24 h, the cells were subjected to luciferase assays. Bars show the fold change in the luciferase activity relative to the value induced by AR without DHT. The data represent the means ± S.D. of three independent experiments. $^{*}P < 0.01$.

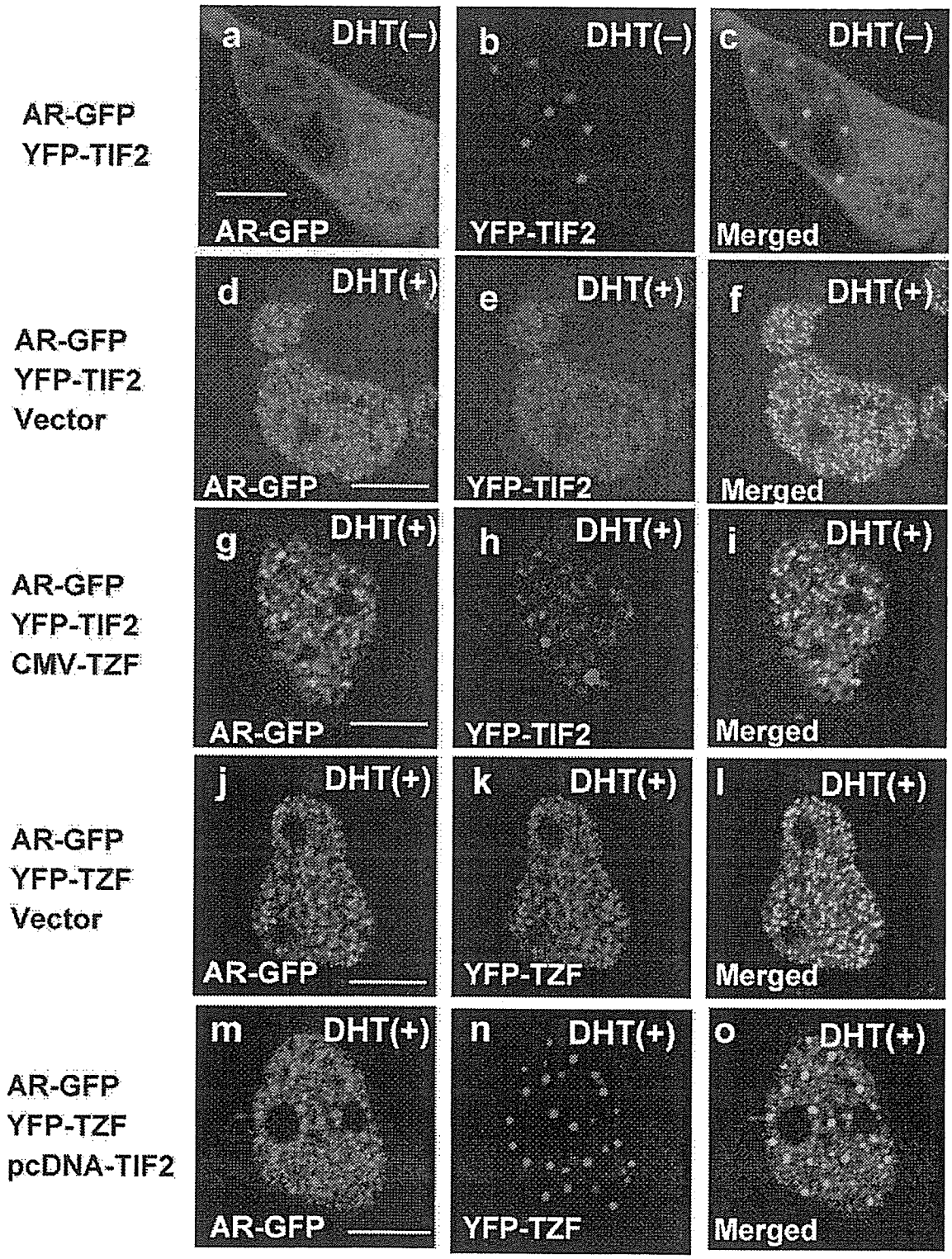

Fig. 9. Imaging analysis of the effects of TZF and TIF2 on the intranuclear foci formation of agonist-bound AR. (a–i) TZF releases TIF2 from intranuclear AR foci. COS-7 cells were transfected with 1 μg of pAR-GFP and 1.5 μg of pEYFP-TIF2 with (g–i) or without (a–f) 3 μg of pFLAG-CMV2-TZF, and incubated for 24 h. Prior to observation, the cells were incubated with (d–i) or without (a–c) 10 nM DHT for 1 h. Fluorescent signals were collected by a laser confocal microscope. AR signals (green; a, d and g), TIF2 signals (red; b, e and h) and merged signals (right; c, f and i) are shown. (j–o) TIF2 releases TZF from intranuclear AR foci. COS-7 cells were transfected with 1 μg of pAR-GFP and 2.2 μg of pEYFP-TZF with (m–o) or without (j–l) 3 μg of pcDNA-TIF2, and incubated for 24 h. After incubation with DHT for 1 h, the cells were observed by laser confocal microscopy. AR signals (green; j and m), TZF signals (red; k and n) and merged signals (right; l and o) are shown. Bars = 5 μm (for interpretation of the references to colour in this figure legend, the reader is referred to the web version of the article).

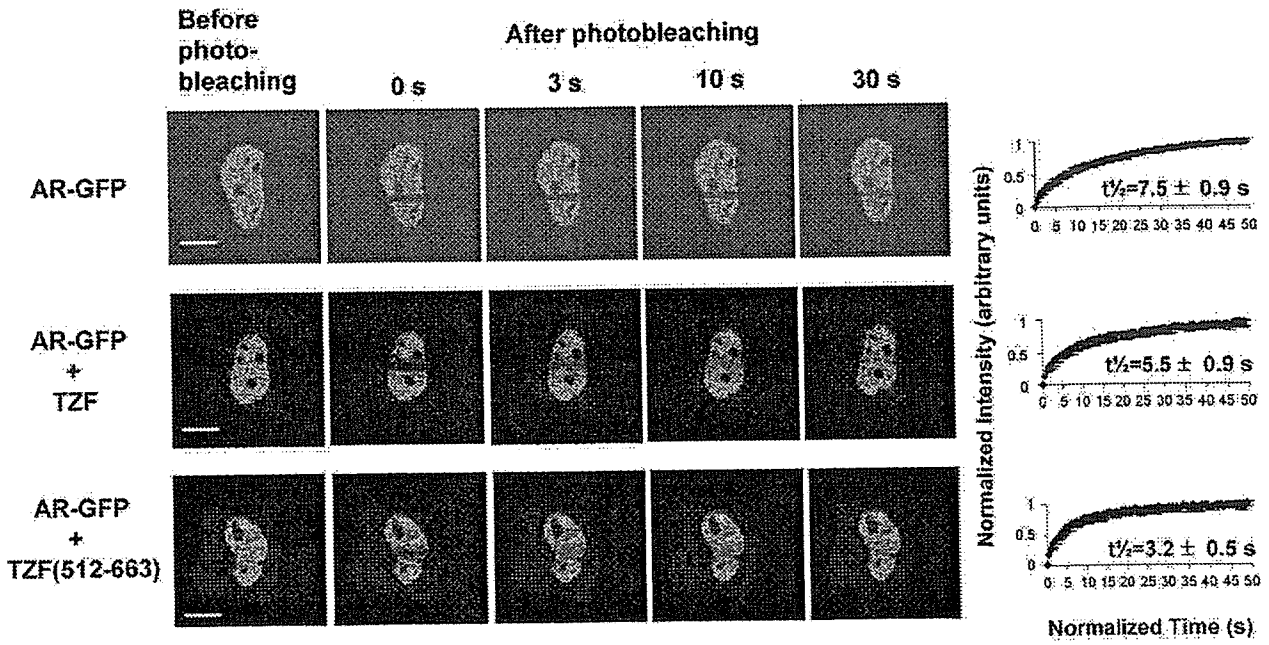

Fig. 10. Intranuclear mobility of AR coexpressed with or without TZF and TZF(512–663). COS-7 cells were transiently transfected with 1 μg of pAR-GFP alone (upper panels), 1 μg of pAR-GFP with 5 μg of pFLAG-CMV2-TZF (middle panels) or 1 μg of pAR-GFP with 5 μg of pFLAG-CMV2-TZF(512–663) (lower panels) as indicated. After incubation for 24 h, the cells were treated with 10 nM DHT for 1 h and subjected to FRAP analyses using a laser scanning microscope. A region of interest (ROI) in the nucleus was photobleached, and images were obtained before and at the indicated time points after the photobleaching. Bars = 5 μm. Graphs in the right panels show the recovery curves of the relative intensities in the photobleached ROI. The values of the half-recovery time ($t_{1/2}$) are expressed as means ± S.D. ($n = 15$).

are particularly abundant in eukaryotic proteomes and play an important role in biological processes, including protein–protein interactions (Liu et al., 2002; Liu and Rost, 2003). Therefore, further mutational analyses of TZF are necessary to identify the critical amino acid residues required for the repression of AR-mediated transactivation.

We applied the modified mammalian one-hybrid assay for detecting interactions of AR with the full-length TZF and its truncated mutants (Fig. 3). In this assay, expression of the TZF corepressor might cause an inhibition of basal AR-mediated transactivation. However, coexpression of AR with VP-16-fused TZF and its mutants induced strong transactivations due to the interaction between AR and TZF. These strong transactivations are thought to overcome the inhibitory effect by TZF.

Previous RT-PCR analyses revealed that TZF was highly expressed in the testes and moderately expressed in the prostate, adrenal glands, muscle, kidneys and uterus. During testicular development in mice, elevated expression of TZF was restricted to spermatocytes at the pachytene stage of meiotic prophase and to both round and elongated spermatids (Inoue et al., 2000; Ishizuka et al., 2003). This tissue- and stage-specific expression of TZF may indicate that TZF negatively regulates the actions of AR during development. However, the functions of TZF in vivo have not yet been clarified. Generation of *tzf*-deficient mice should provide strong clues toward elucidating the roles of TZF in developmental and physiological processes.

After ligand-binding, AR is translocated from the cytoplasm into the nucleus, where it activates the transcription of its target genes while simultaneously forming subnuclear foci (Tomura et al., 2001). This ligand-induced foci formation is commonly observed in steroid hormone receptors, such as glucocorticoid receptor (Ogawa et al., 1995), mineralocorticoid receptor (Fejes-Tóth et al., 1998), estrogen receptor-α (Stenoien et al., 2000; Htun et al., 1999) and vitamin D receptor (Racz and Barsony, 1999). Many pieces of evidence have accumulated indicating that this foci formation is closely linked to their transcriptional activation functions (Fejes-Tóth et al., 1998; Stenoien et al., 2000; Tomura et al., 2001; Saitoh et al., 2002). The present study provides another example, since GFP-TZF(512–663) was redistributed and colocalized with AR-CFP after addition of DHT, but distinct (complete) foci formation of AR-CFP was inhibited (Fig. 7E), reflecting the strong corepressor effect of TZF(512–663). However, quantitative analyses have hardly been carried out because it is difficult to count the numbers of intranuclear foci of steroid hormone receptors. We recently developed a three-dimensional imaging method that enables quantification of the numbers of intranuclear foci of steroid hormone receptors (Tomura et al., 2001; Saitoh et al., 2002). In the present study, the number of AR foci and AR-mediated transactivation were directly compared, and a clear correlation between these two factors was revealed (Fig. 8). N-CoR and SMRT are well-characterized corepressors that are thought to interact with nuclear receptors in the absence of a ligand or the presence of antagonists and confer transcriptional repression (Heinlein and Chang, 2002; Jones and Shi, 2003; Privalsky, 2004). However, AR was recently reported to be able to bind N-CoR and SMRT even in the presence of agonists (Cheng et al., 2002; Liao et al.,

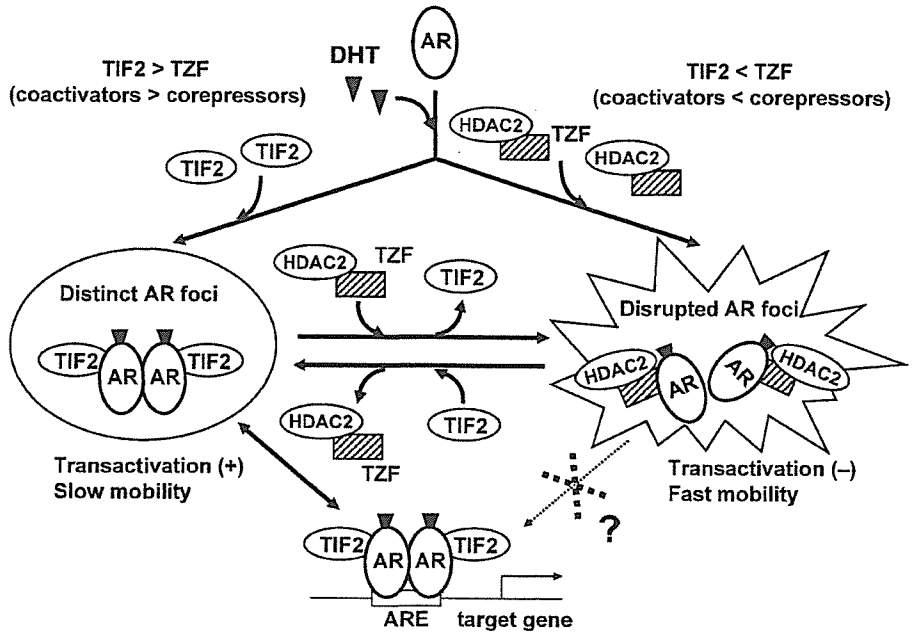

Fig. 11. An equilibrium model for intranuclear AR foci formation modulated by coregulators. The ratio of coactivators/corepressors expressed in a cell is presumed to determine the number of intranuclear foci and the transactivation activity of AR. Under the intranuclear condition where the content of corepressors such as TZF is considerably lower than that of coactivators, agonist-bound AR recruits coactivators and forms a transcriptionally active conformation, which is coupled with transfer to proper subnuclear compartments (distinct AR foci). AR foci formation is parallel to the transcription function and slow mobility. Agonist-bound AR in these proper compartments undergoes rapid exchange between the compartments and transcription sites of the target genes and is able to activate transcription. Under the condition where the content of corepressors is relatively higher than that of coactivators, the corepressors with HDAC bind to liganded AR, resulting in impairment of foci formation (disrupted AR foci). Agonist-bound AR in impaired compartments showed reduced transcriptional activation and fast mobility. It can be speculated that AR in the impaired foci might not have proper access to the transcription sites.

2003), and competition for agonist-bound AR between corepressors and coactivators was suggested to be the mechanism of the repression (Liao et al., 2003). A similar mechanism could be suggested for TZF-mediated repression of AR-induced transactivation, since the AR-mediated transactivation function varied depending on the TZF(512–663)/TIF2 ratio (Fig. 8B), while TZF was recruited by AR ligand-dependently, but also impaired complete foci formation of AR and dissociated the coactivator TIF2 from the AR foci (Fig. 9). However, an increase in TIF2 dissociated TZF and recovered the distinct foci formation of AR (Fig. 8A).

The FRAP analysis revealed that coexpression of full-length TZF or its mutants increased the intranuclear mobility of AR. Coexpression of TZF(512–663), which strongly repressed AR-mediated transcription, led to a higher mobility of AR compared to that of full-length TZF. The half-recovery time of AR would be correlated with its transcriptional activity. Previous studies revealed that ligand-bound steroid hormone receptors interact with the nuclear matrix, resulting in their decreased mobility (Fejes-Tóth et al., 1998; Htun et al., 1999; Schaaf and Cidlowski, 2003). TZF protein may inhibit the binding of AR to the nuclear matrix and cause a diffuse distribution of AR in the nucleus.

Our present results indicate that the ligand-dependent transactivation function of AR is quantitatively correlated with its foci formation, and that corepressors such as TZF act on these intranuclear events competitively with coactivators. Furthermore, the current results may suggest that competition with coactivators is a common repression mechanism for corepressors of agonist-bound AR, such as N-CoR, SMRT and TZF. Fig. 11 summarizes the speculated action of TZF based on the present findings.

Acknowledgements

We are grateful to Mitoshi Toki for his technical assistance in performing the three-dimensional imaging analyses. This work was supported in part by grants-in-aid for Scientific Research (B) and Exploratory Research and a grant for the 21st Century Center of Excellence (COE) Program (Kyushu University) from the Ministry of Education, Culture, Sports, Science and Technology, Japan.

References

Adachi, M., Takayanagi, R., Tomura, A., Imasaki, K., Kato, S., Goto, K., Yanase, T., Ikuyama, S., Nawata, H., 2000. Androgen-insensitivity syndrome as a possible coactivator disease. N. Engl. J. Med. 343, 856–862.

Aranda, A., Pascual, A., 2001. Nuclear hormone receptors and gene expression. Physiol. Rev. 81, 1269–1304.

Brinkmann, A.O., 2001. Molecular basis of androgen insensitivity. Mol. Cell. Endocrinol. 179, 105–109.

Cheng, S., Brzostek, S., Lee, S.R., Hollenberg, A.N., Balk, S.P., 2002. Inhibition of the dihydrotestosterone-activated androgen receptor by nuclear receptor corepressor. Mol. Endocrinol. 16, 1492–1501.

Fejes-Tóth, G., Pearce, D., Náray-Fejes-Tóth, A., 1998. Subcellular localization of mineralocorticoid receptors in living cells: effects of receptor agonists and antagonists. Proc. Natl. Acad. Sci. U.S.A. 95, 2973–2978.

Gelmann, E.P., 2002. Molecular biology of the androgen receptor. J. Clin. Oncol. 20, 3001–3015.

Gobinet, J., Poujol, N., Sultan, Ch., 2002. Molecular action of androgens. Mol. Cell. Endocrinol. 198, 15–24.

Gottlieb, B., Pinsky, L., Beitel, L.K., Trifiro, M., 1999. Androgen insensitivity. Am. J. Med. Genet. 89, 210–217.

Heinlein, C.A., Chang, C., 2002. Androgen receptor (AR) coregulators: an overview. Endocr. Rev. 23, 175–200.

Heinzel, T., Lavinsky, R.M., Mullen, T.M., Soderstrom, M., Laherty, C.D., Torchia, J., Yang, W.M., Brard, G., Ngo, S.D., Davie, J.R., Seto, E., Eisenman, R.N., Rose, D.W., Glass, C.K., Rosenfeld, M.G., 1997. A complex containing N-CoR, mSin3 and histone deacetylase mediates transcriptional repression. Nature 387, 43–48.

Htun, H., Holth, L.T., Walker, D., Davie, J.R., Hager, G.L., 1999. Direct visualization of the human estrogen receptor alpha reveals a role for ligand in the nuclear distribution of the receptor. Mol. Biol. Cell 10, 471–486.

Hu, X., Li, Y., Lazar, M.A., 2001. Determinants of CoRNR-dependent repression complex assembly on nuclear hormone receptors. Mol. Cell. Biol. 21, 1747–1758.

Inoue, A., Ishiji, A., Kasagi, S., Ishizuka, M., Hirose, S., Baba, T., Hagiwara, H., 2000. The transcript for a novel protein with a zinc finger motif is expressed at specific stages of mouse spermatogenesis. Biochem. Biophys. Res. Commun. 273, 398–403.

Ishizuka, M., Ohshima, H., Tamura, N., Nakada, T., Inoue, A., Hirose, S., Hagiwara, H., 2003. Molecular cloning and characteristics of a novel zinc finger protein and its splice variant whose transcripts are expressed during spermatogenesis. Biochem. Biophys. Res. Commun. 301, 1079–1085.

Ishizuka, M., Kawate, H., Takayanagi, R., Ohshima, H., Tao, R.-H., Hagiwara, H., 2005. A zinc finger protein TZF is a novel corepressor of androgen receptor. Biochem. Biophys. Res. Commun. 331, 1025–1031.

Jones, P.L., Shi, Y.-B., 2003. N-CoR-HDAC corepressor complexes: roles in transcriptional regulation by nuclear hormone receptors. Curr. Top. Microbiol. Immunol. 274, 237–268.

Kawano, H., Sato, T., Yamada, T., Matsumoto, T., Sekine, K., Watanabe, T., Nakamura, T., Fukuda, T., Yoshimura, K., Yoshizawa, T., Aihara, K., Yamamoto, Y., Nakamichi, Y., Metzger, D., Chambon, P., Nakamura, K., Kawaguchi, H., Kato, S., 2003. Suppressive function of androgen receptor in bone resorption. Proc. Natl. Acad. Sci. U.S.A. 100, 9416–9421.

Kawate, H., Wu, Y., Ohnaka, K., Nawata, H., Takayanagi, R., 2005. Tob proteins suppress steroid hormone receptor-mediated transcriptional activation. Mol. Cell. Endocrinol. 230, 77–86.

Kinyamu, H.K., Archer, T.K., 2004. Modifying chromatin to permit steroid hormone receptor-dependent transcription. Biochim. Biophys. Acta 1677, 30–45.

Liao, G., Chen, L.Y., Zhang, A., Godavarthy, A., Xia, F., Ghosh, J.C., Li, H., Chen, J.D., 2003. Regulation of androgen receptor activity by the nuclear receptor corepressor SMRT. J. Biol. Chem. 278, 5052–5061.

Liu, J., Rost, B., 2003. NORSp: predictions of long regions without regular secondary structure. Nucleic Acids Res. 31, 3833–3835.

Liu, J., Tan, H., Rost, B., 2002. Loopy proteins appear conserved in evolution. J. Mol. Biol. 322, 53–64.

Mangelsdorf, D.J., Thummel, C., Beato, M., Herrlich, P., Schütz, G., Umesono, K., Blumberg, B., Kastner, P., Mark, M., Chambon, P., Evans, R.M., 1995. The nuclear receptor superfamily: the second decade. Cell 83, 835–839.

Ogawa, H., Inouye, S., Tsuji, F.I., Yasuda, K., Umesono, K., 1995. Localization, trafficking, and temperature-dependence of the Aequorea green fluorescent protein in cultured vertebrate cells. Proc. Natl. Acad. Sci. U.S.A. 92, 11899–11903.

Ogryzko, V.V., Schiltz, R.L., Russanova, V., Howard, B.H., Nakatani, Y., 1996. The transcriptional coactivators p300 and CBP are histone acetyltransferases. Cell 87, 953–959.

Privalsky, M.L., 2004. The role of corepressors in transcriptional regulation by nuclear hormone receptors. Annu. Rev. Physiol. 66, 315–360.

Racz, A., Barsony, J., 1999. Hormone-dependent translocation of vitamin D receptors is linked to transactivation. J. Biol. Chem. 274, 19352–19360.

Roy, A.K., Lavrovsky, Y., Song, C.S., Chen, S., Jung, M.H., Velu, N.K., Bi, B.Y., Chatterjee, B., 1999. Regulation of androgen action. Vitam. Horm. 55, 309–352.

Saitoh, M., Takayanagi, R., Goto, K., Fukamizu, A., Tomura, A., Yanase, T., Nawata, H., 2002. The presence of both the amino- and carboxyl-terminal domains in the AR is essential for the completion of a transcriptionally active form with coactivators and intranuclear compartmentalization common to the steroid hormone receptors: a three-dimensional imaging study. Mol. Endocrinol. 16, 694–706.

Schaaf, M.J.M., Cidlowski, A., 2003. Molecular determinants of glucocorticoid receptor mobility in living cells: the importance of ligand affinity. Mol. Cell. Biol. 23, 1922–1934.

Stenoien, D.L., Mancini, M.G., Patel, K., Allegretto, E.A., Smith, C.L., Mancini, M.A., 2000. Subnuclear trafficking of estrogen receptor-alpha and steroid receptor coactivator-1. Mol. Endocrinol. 14, 518–534.

Stenoien, D.L., Patel, K., Mancini, M.G., Dutertre, M., Smith, C.L., O'Malley, B.W., Mancini, M.A., 2001. FRAP reveals that mobility of oestrogen receptor-alpha is ligand- and proteasome-dependent. Nat. Cell. Biol. 3, 15–23.

Tomura, A., Goto, K., Morinaga, H., Nomura, M., Okabe, T., Yanase, T., Takayanagi, R., Nawata, H., 2001. The subnuclear three-dimensional image analysis of androgen receptor fused to green fluorescence protein. J. Biol. Chem. 276, 28395–28401.

Webb, P., Anderson, C.M., Valentine, C., Nguyen, P., Marimuthu, A., West, B.L., Baxter, J.D., Kushner, P.J., 2000. The nuclear receptor corepressor (N-CoR) contains three isoleucine motifs (I/LXXII) that serve as receptor interaction domains (IDs). Mol. Endocrinol. 14, 1976–1985.

Yanase, T., Adachi, M., Goto, K., Takayanagi, R., Nawata, H., 2004. Coregulator-related diseases. Intern. Med. 43, 368–373.

Yeh, S., Tsai, M.Y., Xu, Q., Mu, X.M., Lardy, H., Huang, K.E., Lin, H., Yeh, S.D., Altuwaijri, S., Zhou, X., Xing, L., Boyce, B.F., Hung, M.C., Zhang, S., Gan, L., Chang, C., 2002. Generation and characterization of androgen receptor knockout (ARKO) mice: an in vivo model for the study of androgen functions in selective tissues. Proc. Natl. Acad. Sci. U.S.A. 99, 13498–13503.

Available online at www.sciencedirect.com
SCIENCE DIRECT®
ELSEVIER
Biochemical and Biophysical Research Communications 341 (2006) 515–521
BBRC
www.elsevier.com/locate/ybbrc

Opposite effects of alternative TZF spliced variants on androgen receptor

Rong-Hua Tao [a], Hisaya Kawate [a], Keizo Ohnaka [a], Masamichi Ishizuka [b], Hiromi Hagiwara [b], Ryoichi Takayanagi [a,*]

[a] *Department of Geriatric Medicine, Graduate School of Medical Sciences, Kyushu University, Maidashi 3-1-1, Higashi-ku, Fukuoka 812-8582, Japan*
[b] *Department of Biomedical Engineering, Toin University of Yokohama, Kurogane-cho 1614, Aoba-ku, Yokohama 225-8502, Japan*

Received 28 December 2005
Available online 13 January 2006

Abstract

We previously demonstrated that testicular zinc-finger protein (TZF) was a corepressor of the androgen receptor (AR). In the present study, we further showed that TZF-L, an alternative spliced variant of TZF, enhanced transactivation function of AR. Deletion analysis of TZF-L revealed that its N-terminus, which almost corresponded to that of TZF, but not its C-terminus was able to interact with AR. Additional analysis suggested that TZF and TZF-L were able to form both homodimers and heterodimers. TZF-L inhibited the homodimer formation of TZF and the intranuclear dot formation of TZF. We propose that in the unique regulation system of AR-mediated transactivation, two spliced isoforms of TZF act as coactivator and corepressor, respectively.
© 2006 Elsevier Inc. All rights reserved.

Keywords: Androgen receptor; Transcription; Coregulator; GFP

Androgens play essential roles in the expression of the male phenotype through the androgen receptor (AR). AR is a member of the nuclear receptor (NR) superfamily, which generally functions as a ligand-dependent transcriptional factor [1,2]. AR is located in the cytoplasm before ligand binding and becomes translocated into the nucleus upon ligand binding to recognize androgen responsive elements of target genes, resulting in transcriptional activation or repression [1,3,4]. We previously reported that AR formed intranuclear fine foci in a ligand-dependent manner [5,6]. NR-mediated transcription is known to be regulated by two types of cofactors, coactivators and corepressors. To date, a large number and a wide variety of coactivators and corepressors of NR-mediated transactivation have been identified [7,8].

TZF (testicular zinc-finger protein) consists of 942 amino acid residues and carries a Cys_2-His_2 type of zinc-finger motif at the C-terminal end of the protein [9]. TZF-L has been identified as an alternative spliced variant of TZF. It has 2025 amino acid residues, and the N-terminal 902 amino acids of TZF-L protein are identical to those of TZF [10]. TZF-L has two zinc-finger motifs of the Cys_2-His_2 type, one of which is common with that of TZF. Both TZF and TZF-L are highly expressed in testes and moderately in kidneys and ovaries. We previously reported that TZF repressed AR-mediated transcriptional activation by interacting with the N-terminus of AR [11]. TZF forms intranuclear dots and is recruited into AR foci after treatment of the ligand.

In the present study, we investigated effects of TZF-L on AR-mediated transactivation function. In contrast with TZF, TZF-L enhanced AR-mediated transcriptional activation. The N-terminus of TZF-L, which almost corresponds to TZF, was able to interact with AR. We also indicated that TZF and TZF-L formed both homodimers and heterodimers. These two spliced variants of TZF may have unique regulation mechanisms for AR-mediated transcriptional activation.

* Corresponding author. Fax: +81 92 642 6911.
E-mail address: takayana@geriat.med.kyushu-u.ac.jp (R. Takayanagi).

Materials and methods

Plasmid constructs. Expression plasmids for AR, pCMV-hAR, and firefly reporter plasmids (pGL3-MMTV and pGL3-PSA) were prepared as previously described [5,11,12]. Expression plasmids for TZF-L, pLP-EGFP-C1-TZF-L [10] were digested with *Sal*I and *Xho*I restriction enzymes to obtain a *Sal*I–*Xho*I fragment encoding the C-terminus of TZF-L, and a *Sal*I fragment encoding the remaining portion of TZF-L. The *Sal*I–*Xho*I fragment was first inserted into the *Sal*I site of both pEGFP-C1 and pEYFP-C1 vectors (BD Sciences Clontech, Palo, Alto, CA), followed by insertion of the *Sal*I fragment into the *Sal*I site of the same vector to produce pEGFP-TZF-L and pEYFP-TZF-L, respectively. Similarly, another expression plasmid for TZF-L, pFLAG-CMV2-TZF-L, was constructed using pFLAG-CMV2 vector (Sigma–Aldrich, St. Louis, MO). An expression plasmid for the N-terminus (amino acids 1–902) of TZF-L, pEGFP-TZF-L-N, was constructed as follows: a fragment encoding 758–902 amino acid residues of TZF-L was amplified by PCR from pLP-EGFP-C1-TZF-L, using the following set of oligonucleotide primers: TZF-L-N-5 (5′-GTGAGTCGACTTCAGGAT-3′) and TZF-L-N-3 (5′-CCGCTCGAGCTGTGTGTGCTTCTTATTGTGC-3′). The PCR-amplified fragment was cloned into pCR-Blunt II-TOPO vector (Invitrogen Corp., Carlsbad, CA), and the *Sal*I–*Xho*I fragment encoding TZF-L (amino acids 758–902) was subcloned into the *Sal*I site of pEGFP-C1 vector, followed by insertion of the *Sal*I fragment encoding the N-terminus (amino acids 1–758) of TZF-L into the *Sal*I site. To construct an expression plasmid for TZF-L-C (amino acids 902–2025), pEGFP-TZF-L-C, a fragment encoding amino acid residues 902–1171 of TZF-L was amplified by PCR from pLP-EGFP-C1-TZF-L using the following set of primers: TZF-L-C-5 (5′-CCGCTCGAGAGACACTGGATCCCTAC AAC-3′) and TZF-L-C-3 (5′-AACCTGACTTGCGGAGTACTG-3′). The PCR-amplified fragment was cloned into pCR-Blunt II-TOPO vector, and then an *Xho*I–*Eco*RI fragment encoding TZF-L (amino acids 902–1171) was subcloned into the *Xho*I and *Eco*RI sites of pEGFP-C1 vector, followed by insertion of the *Sca*I–*Xho*I fragment of pLP-EGFP-C1-TZF-L encoding the C-terminus (amino acids 1171–2025) of TZF-L into the *Sca*I and *Sal*I sites. The TZF cDNA fragment was subcloned into pFLAG-CMV2 and pEGFP-C1, resulting in pFLAG-CMV2-TZF and pEGFP-C1-TZF, respectively.

For the mammalian two-hybrid assay, pEGFP-TZF-L was digested with *Sma*I, and a *Sma*I fragment containing TZF-L cDNA was inserted into blunt-ended *Bam*HI sites of pBIND and pACT vectors (Promega, Madison, WT), to produce pBIND-TZF-L and pACT-TZF-L, respectively. Expression plasmids for TZF-L-C, pBIND-TZF-L-C, and pACT-TZF-L-C were constructed by inserting the *Xho*I–*Sma*I fragment from pEGFP-TZF-L-C into *Sal*I- and *Eco*RV-digested pBIND, and pACT vectors, respectively. Expression plasmids for TZF-L-N, pBIND-TZF-L-N, and pACT-TZF-L-N were constructed by inserting a *Kpn*I fragment from pEGFP-TZF-L-N into *Kpn*I sites of pBIND and pACT vectors. The cDNA fragment of TZF was subcloned into pBIND and pACT vectors to produce pBIND-TZF and pACT-TZF, respectively. Expression plasmid for AR, pACT-AR, was prepared as previously described [13]. Validity of the structure of all constructs was confirmed by DNA sequencing.

Cell culture. The monkey kidney-derived cell line COS-7 was obtained from the Riken Cell Bank (Tokyo, Japan). The human prostatic cancer cell line PC3 and the mouse fibroblast cell line NIH3T3 were obtained from the American Type Culture Collection (Manassas, VA). COS-7 and NIH3T3 cells were maintained in Dulbecco's modified Eagle's medium (DMEM, Sigma), and PC3 cells were maintained in Roswell Park Memorial Institute 1640 medium (Sigma), supplemented with 10 % fetal bovine serum (FBS, Sanko Junyaku, Tokyo, Japan) and 100 U/ml penicillin–streptomycin (Invitrogen).

Functional reporter assay. Cells were cultured in 12-well plates (1×10^5 cells/well), and transfected with 0.3 μg/well pGL3-PSA or pGL3-MMTV as reporter, 2 ng/well pRL-CMV (Renilla Luciferase vector, Promega, Madison, WI) as internal control, and 0.1 μg/well pCMV-hAR together with 0.5 μg/well of the expression plasmid for TZF or TZF-L, using 2.7 μl Superfect Transfection Reagent (Qiagen GmbH, Hilden, Germany). In all co-transfection studies, the total amount of plasmid DNA was fixed by adjusting the transfection mixture with empty vector. After 4-h incubation, cells were rinsed with phosphate-buffered saline (PBS), and re-fed with medium containing 10% charcoal-stripped FBS, in the presence or absence of 10 nM 5α-dihydrotestosterone (DHT). After an additional incubation for 24 h, cells were lysed using lysis buffer supplied with the luciferase kit (Promega), and luciferase activity was assayed using the Dual-Luciferase Reporter Assay System (Promega). Data were expressed as means ± SD of three independent experiments. One-way analysis of variance followed by Scheffé's test was used for multigroup comparisons. A P value <0.05 was considered to be statistically significant.

Mammalian two-hybrid assay. NIH3T3 (1×10^5 cells/well) cells were seeded in 12-well plates at 24 h before transfection. Cells were co-transfected with 0.6 μg pG5*luc* (Promega) as reporter, 0.3 μg pACT-AR and 0.1 μg pBIND-TZF-L, pBIND-TZF-L-N or pBIND-TZF-L-C. The pBIND vector also encoded the *Renilla reniformis* luciferase as internal control. For detection of homodimers and heterodimers, plasmids (pG5*luc*, pACT-TZF, pBIND-TZF, pACT-TZF-L, and pBIND-TZF-L) were used for transfection. Equimolar amounts of the empty vector DNA were added to each well. Following treatment with 10 nM DHT for 24 h, cells were lysed, and luciferase activity was measured as described above.

Co-immunoprecipitation and immunoblot analysis. COS-7 cells (1×10^6 cells/dish) were seeded in 100-mm culture dishes, and transiently transfected with 1.5 μg pCMV-hAR using 7.5 μg pEGFP-TZF-L, 5 μg pEGFP-TZF-L-N, and 5 μg pEGFP-TZF-L-C, followed by 24-h incubation in the presence of 10 nM DHT. Whole cell lysates were prepared by lysing cells in a buffer consisting of 20 mM Hepes–NaOH, pH 7.9, 20% glycerol, 100 mM KCl, 0.2 mM EDTA, 0.5% NP-40, and one tablet of protease inhibitor cocktail (Roche Diagnostics, Tokyo, Japan) for 30 min at 4 °C, followed by brief sonication and centrifugation. Protein concentrations were measured using a BCA protein assay kit (Pierce, Rockford,

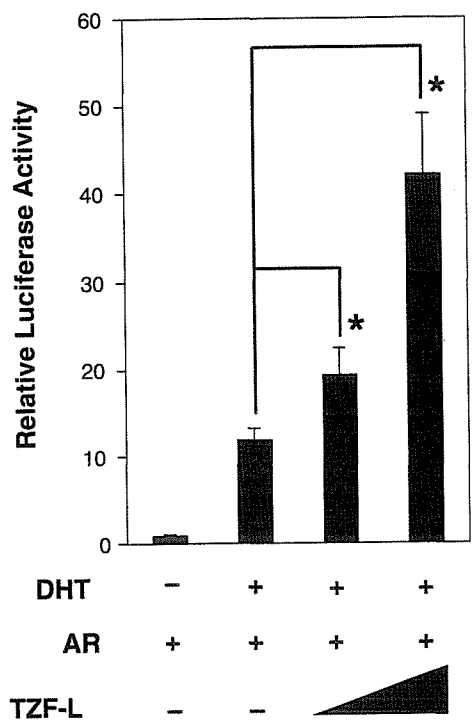

Fig. 1. TZF-L enhances AR-mediated transcriptional activation. PC3 cells were transfected with pGL3-PSA, pRL-CMV, and pCMV-hAR together with or without pFLAG-CMV2-TZF-L as described in Materials and methods. Molar ratios of transfected amounts of pCMV-hAR and pFLAG-CMV2-TZF-L were 1:5 or 1:10. Cells were treated with or without 10 nM DHT for 24 h, and luciferase activity was measured. Bars represent fold changes in luciferase activity relative to the value by AR without DHT. $^*P < 0.01$.

IL), and each protein concentration was adjusted to 1 mg/ml. For the immunoprecipitation assay, antibodies against GFP or AR (C-19, Santa Cruz Biotechnology, Santa Cruz, CA) were pre-incubated with protein A magnetic beads (New England Biolabs, Beverly, MA) at 4 °C for 2 h. Each lysate (200 μg) was incubated with 10 μg anti-GFP or anti-AR antibody-conjugated beads in WB buffer (20 mM Hepes–NaOH, pH 7.9, 20% glycerol, 100 mM KCl, 0.2 mM EDTA, 0.5% NP-40, and 0.5% skim milk) at 4 °C overnight. After the beads were washed three times with 180 μl WB buffer, the bound proteins were eluted in 2 × sodium dodecyl sulfate–polyacrylamide gel electrophoresis (SDS–PAGE) sample buffer (2% SDS, 100 mM dithiothreitol, 60 mM Tris–HCl, pH 6.8, and 0.01% bromophenol blue) and subjected to 10% SDS–PAGE at 20 mA for 5 h. An immunoblot analysis was then performed as previously described [14], using the anti-AR (C-19) antibody for AR, anti-TZF antibody for TZF, and anti-GFP antibody for GFP-fused TZF-L and its mutants.

Confocal laser scanning microscopy. For living cell microscopy, COS-7 cells (2×10^5 cells/dish) were cultured in 35-mm glass-bottomed dishes (Asahi Techno Glass, Tokyo, Japan) and transfected with pEGFP-TZF and/or pEYFP-TZF-L, or pFLAG-CMV2-TZF-L using Superfect reagents (Qiagen). After 3-h incubation, cells were washed with PBS, followed by incubation in DMEM supplemented with 10% charcoal-treated FBS for 16–20 h. Cells were observed with an Axiovert 200 M inverted microscope, equipped with an LSM 510 META scan head (Carl Zeiss, Jena, Germany), and using a 100 × 1.4 numerical aperture oil

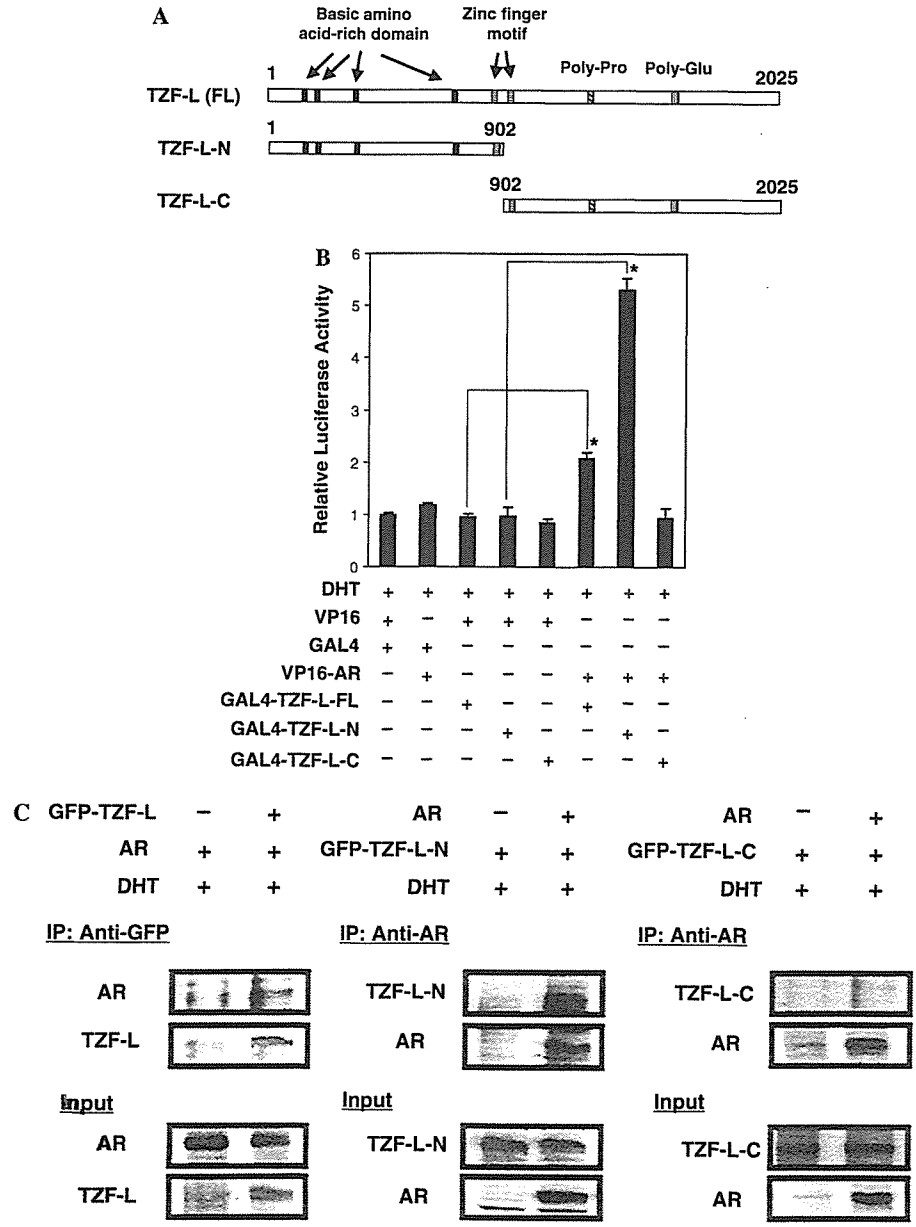

Fig. 2. Identification of the interaction between TZF-L and AR. (A) Schematic representation of full-length TZF-L and its truncated mutants, TZF-L-N and TZF-L-C. (B) A mammalian two-hybrid assay indicated interactions of the full length TZF-L and its N-terminus with AR. NIH3T3 cells were co-transfected with pG5*luc*, pACT-AR, and pBIND-TZF-L, pBIND-TZF-L-N or pBIND-TZF-L-C, and luciferase activities were measured after treatment with 10 nM DHT for 24 h, as described in Materials and methods. Bars represent fold changes in luciferase activity relative to the value by the empty vectors. Data are expressed means ± SD of three independent experiments. $*P < 0.01$. (C) Co-immunoprecipitation analyses of TZF-L and its truncated mutants with AR. COS-7 cells were transfected with pCMV-hAR with pEGFP-TZF-L, pEGFP-TZF-L-N or pEGFP-TZF-L-C and then incubated with 10 nM DHT for 24 h as described in Materials and methods. Whole cell lysates were immunoprecipitated using anti-GFP or anti-AR antibody. Then, precipitates were subjected to immunoblot analysis using the anti-AR antibody for detection of AR, and the anti-GFP antibody for detections of TZF-L, TZF-L-N, and TZF-L-C. Whole cell lysates were also subjected to immunoblot analysis to confirm expressions of AR, TZF-L, TZF-L-N, and TZF-L-C.

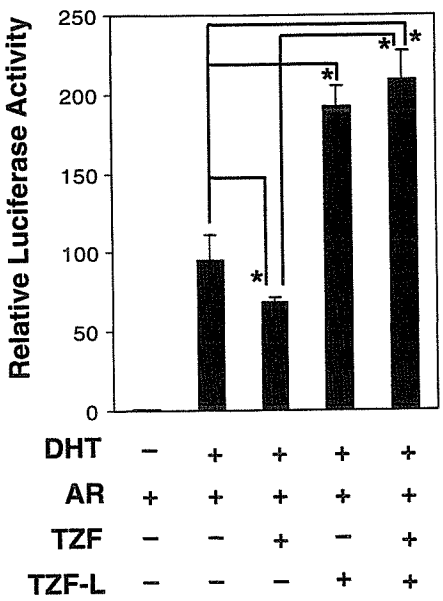

Fig. 3. TZF-L abrogates the repressive function of TZF on AR transactivation. COS-7 cells were transfected with pGL3-MMTV, pRL-CMV, pCMV-hAR, and the expression vector for TZF and/or TZF-L at equimolar amounts, and luciferase activity was measured after treatment with 10 nM DHT for 24 h as described in Materials and methods. Bars represent fold changes in luciferase activity relative to the value by AR without DHT. Data are represented means ± SD of three independent experiments. $*P < 0.01$.

immersion objective as described previously [14,15]. Images were collected at a 12-bit depth resolution of intensities over 1024 × 1024 pixels. For excitation of GFP and YFP, 488-nm argon lasers were employed, and emission signals were separated using the Emission Fingerprinting technique established by Carl Zeiss.

Results

TZF-L enhances AR-mediated transcriptional activation

We previously reported that TZF repressed AR-mediated transcriptional activation [11]. We also isolated an alternative spliced variant of TZF, TZF-L (2025 amino acid residues), which was much longer than TZF (942 amino acid residues) [10]. Nine hundreds and two N-terminal amino acid residues were common in these two variants. To examine effects of TZF-L on AR-mediated transactivation function, a functional reporter assay was performed using a PSA promoter in PC3 cells. Surprisingly, TZF-L enhanced ligand-induced transcriptional activation by AR in a dose-dependent fashion (Fig. 1). Using a different promoter (MMTV) and different cells (COS-7), a similar promoting effect by TZF-L on AR-mediated transactivation was observed (data not shown). These results revealed that, interestingly, TZF-L acted as a coactivator for AR in contrast with the corepressor function of TZF.

The N-terminus of TZF-L interacts with AR

As described previously, the N-terminal 902 amino acid residues of TZF-L were identical to those of TZF, which directly interacted with AR [11]. To examine the interaction of TZF-L with AR, a mammalian two-hybrid assay was performed using the full-length TZF-L and its deletion mutants, TZF-L-N and TZF-L-C, with AR (Fig. 2A). As shown in Fig. 2B, expressions of TZF-L and TZF-L-N but not of TZF-L-C showed higher activities compared to that of the negative control, demonstrating that TZF-L was able to interact with AR through its N-terminal domain. To further confirm the interaction of TZF-L with AR, immunoprecipitation analyses using AR with TZF-L or its mutants were carried out. As shown in Fig. 2C, AR was co-immunoprecipitated with full-length TZF-L and TZF-L-N, but not with TZF-L-C.

TZF-L completely abrogates the repression function of TZF on AR-mediated transactivation

TZF and TZF-L are alternative spliced proteins derived from one gene and are expressed in the same tissues and stages of spermatogenesis [10]. Such a pair of proteins often cooperates to regulate the same physiological processes. Here, we investigated effects of coexpression of these two proteins on AR-mediated transactivation. As shown in Fig. 3, TZF and TZF-L showed opposite effects on AR-mediated transactivation. Coexpression of TZF and TZF-L proteins promoted transactivation by AR to the same level as TZF-L alone. These results indicated that the suppressive effect of TZF

Fig. 4. Homo- and heterodimerization of TZF and TZF-L. (A) TZF forms homodimers and heterodimers with TZF-L. NIH3T3 cells were co-transfected with 0.6 μg pG5*luc*, 0.1 μg pBIND-TZF, and 0.3 μg pACT-TZF-L, pACT-TZF-L-N, or pACT-TZF-L-C. (B) Homodimerization of TZF is inhibited by TZF-L. NIH3T3 cells were transiently co-transfected with 0.3 μg pG5*luc*, 0.1 μg pBIND-TZF, and 0.2 μg pACT-TZF together with or without 1 μg pFLAG-CMV2-TZF or an equimolar amount of pFLAG-CMV2-TZF-L. (C) TZF-L forms homodimers. NIH3T3 cells were transiently co-transfected with 0.6 μg pG5*luc*, 3.3 ng pRL-CMV, 0.2 μg pBIND-TZF-L and 0.4 μg pACT-TZF-L. The cells were then incubated for 48 h and the luciferase activities were measured. Bars represent fold changes in luciferase activity relative to the value by the empty vectors. Data are represented means ± SD of three independent experiments. $*P < 0.01$. (D) TZF co-immunoprecipitates with TZF-L. COS-7 cells were transfected with 4 μg pFLAG-CMV2-TZF and 7.5 μg pEGFP-TZF-L or its empty vector. Whole cell lysates were immunoprecipitated using the anti-GFP antibody. Then, the precipitates were subjected to immunoblot analysis using the anti-TZF antibody for detection of TZF, or the anti-GFP antibody for detection of TZF-L. Whole cell lysates were also subjected to immunoblot analysis to confirm expression levels of TZF and GFP-TZF-L. (E) Distributions of TZF and TZF-L in living cells. COS-7 cells were transfected with pEYFP-TZF-L (a), pEGFP-TZF (b), pEGFP-TZF and pFLAG-CMV2-TZF-L (c), and pEYFP-TZF-L and pEGFP-TZF (d–f). After 24-h incubation, cells were observed using a LSM510META laser scanning microscope. For coexpression analysis, each fluorescent signal (d,e) was obtained using the Emission Fingerprinting technique as described in Materials and methods, and merged (f).

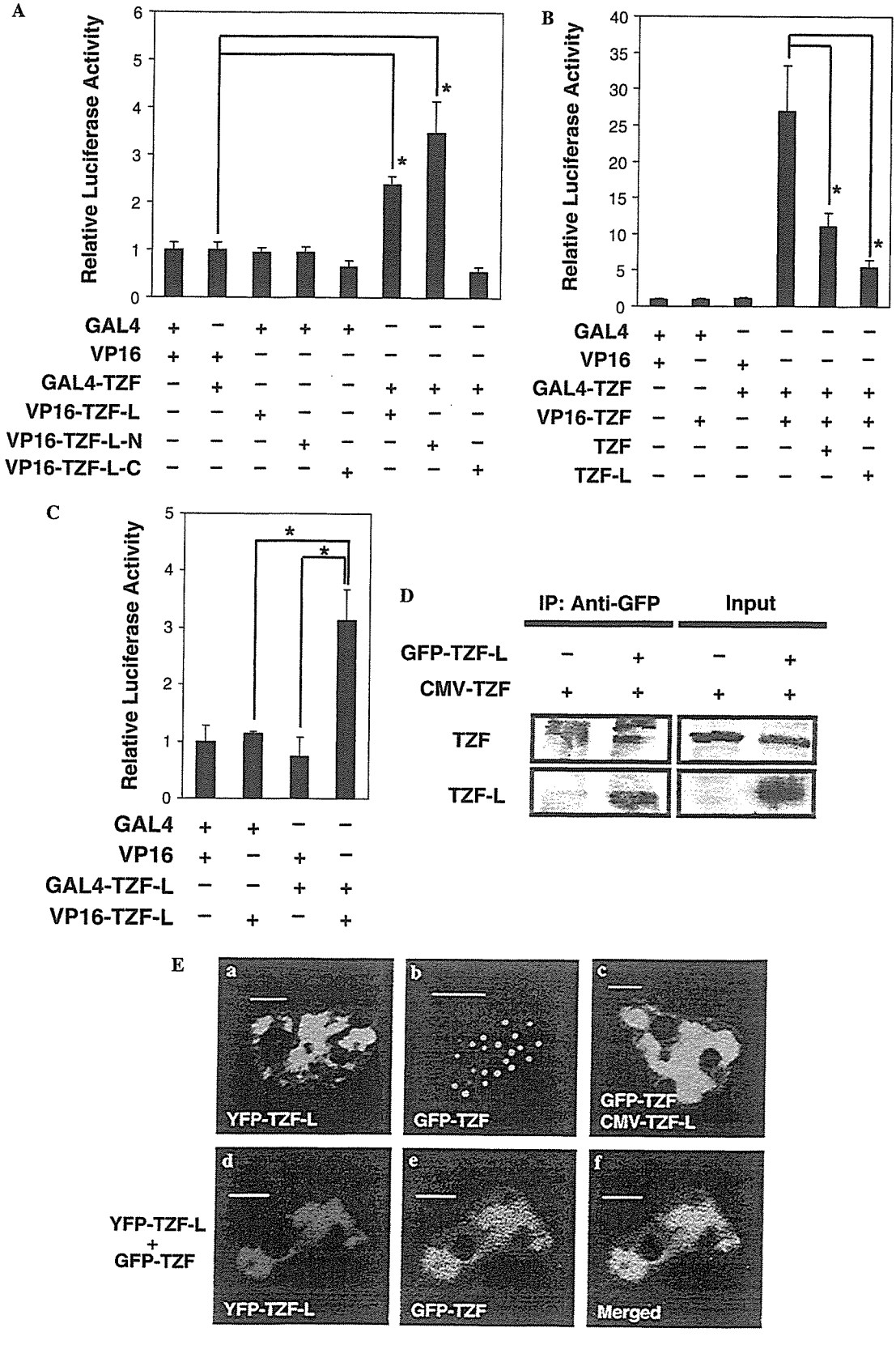
A
Relative Luciferase Activity
GAL4
VP16
GAL4-TZF
VP16-TZF-L
VP16-TZF-L-N
VP16-TZF-L-C
B
Relative Luciferase Activity
GAL4
VP16
GAL4-TZF
VP16-TZF
TZF
TZF-L
C
Relative Luciferase Activity
GAL4
VP16
GAL4-TZF-L
VP16-TZF-L
D
IP: Anti-GFP
Input
GFP-TZF-L
CMV-TZF
TZF
TZF-L
E
YFP-TZF-L
GFP-TZF
GFP-TZF
CMV-TZF-L
YFP-TZF-L
+
GFP-TZF
YFP-TZF-L
GFP-TZF
Merged

on AR-mediated transactivation was completely abrogated by coexpression of TZF-L.

TZF and TZF-L can form both homodimers and heterodimers

Abrogation of the TZF function by TZF-L made us wonder whether these two variants directly interacted with each other. To clarify this matter, a mammalian two-hybrid assay was performed. TZF was able to interact with full-length TZF-L and TZF-L-N, but not with TZF-L-C (Fig. 4A), indicating that TZF-L would form a heterodimer with TZF through its N-terminus. Further investigations suggested that TZF was able to form homodimers, which were strongly inhibited by coexpressing TZF and TZF-L (Fig. 4B). We also found that TZF-L formed homodimers (Fig. 4C). To confirm the interaction between TZF and TZF-L, a co-immunoprecipitation analysis was performed. TZF immunoprecipitated in the presence of anti-GFP antibody, only if GFP-TZF-L was coexpressed (Fig. 4D). Furthermore, we analyzed intracellular localizations of TZF and TZF-L using fluorescent proteins. As we previously reported, TZF formed discrete dots in the nucleus, whereas TZF-L seemed to be distributed at the euchromatin region (Figs. 4E, a and b) [10]. When GFP-TZF was coexpressed with non-fluorescent TZF-L, the intranuclear dots of TZF disappeared, and TZF showed the same intranuclear pattern as TZF-L, indicating that TZF was recruited to where TZF-L existed (Fig. 4E, c). Colocalization of TZF and TZF-L was confirmed using GFP-TZF and YFP-TZF-L (Figs. 4E, d–f). These data indicated that TZF and TZF-L formed both homodimers and heterodimers, and TZF-L recruited TZF.

Discussion

The two alternative spliced isoforms TZF and TZF-L showed opposite effects on AR-mediated transactivation as either corepressor or coactivator. We suggested that TZF was able to form not only homodimers but also heterodimers with TZF-L, and TZF-L inhibited homodimer formation of TZF. Furthermore, TZF-L formed homodimers. Based on these results, we propose a regulation mechanism for AR-mediated transactivation in which TZF homodimers act as corepressors, whereas TZF-TZF-L heterodimers and TZF-L homodimers act as coactivators for AR(Fig. 5).

We previously reported that both TZF and TZF-L were expressed at high levels in spermatogenic cells of testes. These results suggested that TZF and TZF-L might act to control gene activity at particular stages of spermatogenesis [10]. These two spliced variants showed similar stage-specific and tissue-specific expression patterns, suggesting that they functioned cooperatively.

TZF carries one zinc-finger motif, while TZF-L has two. The classical zinc-finger motif (C_2H_2-type) is one of the most common structural motifs in eukaryotes [16–18]. It is well

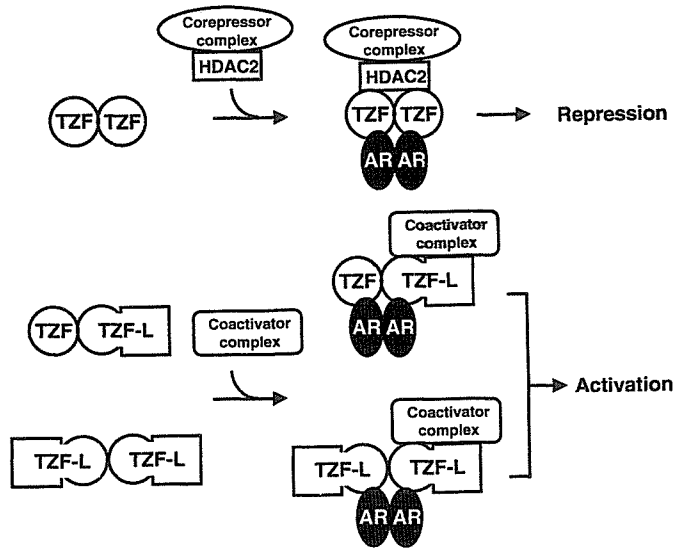

Fig. 5. A model for regulation of AR-mediated transactivation by TZF and TZF-L. Based on our experimental results, we propose a regulation mechanism for AR-mediated transactivation in which TZF homodimers act as corepressors, whereas TZF-TZF-L heterodimers and TZF-L homodimers act as coactivators for AR.

known that most zinc-finger proteins bind to cognate DNA and act as transcription factors. Recent studies revealed that many of these proteins are also able to mediate RNA binding and protein–protein interactions. A homology search for the two C_2H_2 zinc fingers of TZF-L revealed that these motifs were significantly homologous to those of U1 snRNP-specific protein C (U1C) family proteins [19,20]. U1C is critical to the initiation and regulation of pre-mRNA splicing, as a part of the U1 snRNP. In addition to this homology, TZF formed intranuclear dots which were closely located to those found for the splicing factor complex [11]. Based on these evidences, TZF and TZF-L might coordinate the splicing and transcription machineries to regulate nuclear receptor-mediated transactivation functions. Furthermore, U1C was reported to form homodimers through its C_2H_2 zinc-finger motif [21]. The zinc-finger motifs of TZF and TZF-L might also be important for homo- and heterodimerization of these proteins.

In the present study, we found that two alternative spliced variants of TZF had opposite effects on AR-mediated transcriptional activation. Among reported many coregulator proteins, CoAA (coactivator activator) and a short alternatively transcribed isoform, CoAM (coactivator modulator), also showed different actions on steroid hormone receptor-mediated transactivation [22,23]. CoAA, which was identified as a cofactor of thyroid hormone receptor-binding protein (TRBP), acts as a coactivator synergistically with TRBP and CBP [22]. In contrast, CoAM, which carries two RNA recognition motifs but lacks a TRBP-binding domain, completely eliminates synergistic activation effects of both TRBP and CBP. However, it is unclear whether CoAM just removes the CoAA-induced enhancement of the steroid hormone receptor-mediated